Spectral Analysis of Airborne Effluents from Nuclear Facilities and Design of AOTF Spectroradiometer (U)

by
E. Villa
Westinghouse Savannah River Company
Savannah River Site
Aiken, South Carolina 29808
D. R. Suhre

L. H. Taylor

DOE Contract No. **DE-AC09-89SR18035**

DISCLAIMER

DISCLAIMER

Portions of this document may be illegible in electronic image products. Images are produced from the best available original document.

WSRC-TR-95-0136
- AOTFSR7.doc
03/20/95

g3

SPECTRAL ANALYSIS OF AIRBORNE EFFLUENTS FROM NUCLEAR FACILITIES AND DESIGN OF AOTF SPECTRORADIOMETER

Eliel Villa
Savannah River Technology Center

and

D. R. Suhre and L. H. Taylor
Westinghouse Science & Technology Center

TABLE OF CONTENTS

INTRODUCTION AND SUMMARY

This report summarizes the spectral analysis and design of an acousto optic tunable filter (AOTF) imaging spectroradiometer for the project SR003 (Detection of of Airborne Chemicals by AOTF). This system will use passive open-path infrared absorption to detect the presence of various source gases. A thallium arsenic selenide (TAS) AOTF will be used to select the appropriate spectral regions where strong absorbances exist for the gases, and the location of the gas will be displayed on the imaged scene.

Of the 42 known source gases related to nuclear activities, the spectra of 31 gases were found in the Infrared Analysis, Inc., Digitized Reference Library. Eight more spectra were measured as part of this program. Each spectrum was analyzed for a "tag line". A tag line is the highest absorbance line without atmospheric absorption line interferences. Equilibrium vapor concentrations were determined and the absorbance of the tag line scaled to that concentration. The radiance of the plume which is determined by the absorbance and the diameter of the gas plume with the spectroradiometer sensitivity, provides a relative measurement of the detection probability in open path monitoring.

Absorbances of tag lines depend a great deal on the specific gas; the highest value being 2800 times stronger than the lowest value. Equilibrium vapor pressures have an even greater variation -- 3×10^8. Relative detection probabilities of the spectral emissions from the source gases varied over a range of 1.6×10^4 and were dominated by the blackbody radiation dependence on wavelength, which dictated low detection probabilities at wavelengths below 8 μm, and the equilibrium vapor pressure which favored gases with low boiling points. This analysis resulted in the rank ordering of all source gases relative to their probability of detection.

The spectrometer design centered around the TAS AOTF with a 2 cm^{-1} resolution. The 2 cm^{-1} resolution is needed in order to properly differentiate the effluents of interest in a plume. AOTF can be fabricated in two modes called the non-collinear and collinear configurations. A collinear AOTF increases the pathlength of the light interaction with the sound increasing wavelength resolution. The 2 cm-1 resolution can be accomplished with the collinear AOTF but not with a non-collinear configuration. After careful consideration of the risks involved, the design ended up as having two separate AOTFs covering the 2-5 μm and 8-12 μm bands. These separate systems were linked with a common input optical axis, so that a single telescope can be used to change the field of view.

Infrared cameras and other system components were selected or designed according to the system specifications. The field of view of the cameras had to match to the AOTFs, the spectral range had to be consistent with the results of the spectral analysis, and the sensitivities had to be as high as possible.

This search resulted in the selection of an Inframetrics 760 camera for the 8-12 μm region, and a Cincinnati Electronics IRC-160 camera for the 2-5 μm band.

The spectral image data will be recorded in near real time, and then analyzed in-depth. The analysis consists of adding frames and pixels to increase the sensitivity, and then displaying the location of the detected gas on the image. The analysis indicated excellent sensitivities in the 8-12 μm band, with sensitivities as high as 16 ppb-m for such source gases as tributyl phosphate. In the 2-5 μm band, the sensitivity was very poor, which is due mainly to the lack of room temperature thermal radiation below 3.5 μm. Due to the poor sensitivity predictions, along with the scarcity of source gas tag lines in this region, passive open-path monitoring is not nearly as viable in the 2-5 μm band, and it was recommended that the system concentrate only upon the 8-12 μm band.

1. SOURCE SPECTROSCOPY

1.1 GENERAL APPROACH

The goal of the AOTF Spectroradiometer System Program is to demonstrate the applicability of an Imaging Acousto-Optic Tunable Filter (AOTF) to the open path detection of gaseous effluents related to nuclear activities. The optical spectroscopy of the source gases must be known in order to design an optimum system. Gases have spectra which fall into five wavelength regions:[1]

- UV and Visible (0.2 to 0.76 μm). Atoms and homonuclear diatomic molecules have spectra in this region only. Some light molecules also have spectra here.
- Near-IR (0.76 to 3 μm). Most light molecules have spectra here.
- Mid-IR (3 to 6 μm). Most molecules have spectra here but the lines overlap extensively, making it difficult to identify molecular species.
- Far-IR (6 to 15 μm). Richest spectral region for molecular identification.
- Extreme-IR (15 to 1000 μm). Few molecules have important bands here.

Roughly 10% of molecules have spectra useful for identification in the near-IR, 35% in the mid-IR, 80% in the far-IR, and 1% in the extreme-IR.

The chemicals involved in the nuclear operations are fairly well known. They all emit in the infrared region from 2 to 14 μm. We have spectra for the great majority of these gases in a digitized reference library and have measured the spectra for those remaining gases which could be obtained commercially from chemical suppliers.

Each spectrum is analyzed for a "tag line", which is the highest absorbance line with a center which does not overlap any atmospheric absorption line. Equilibrium vapor concentrations are then determined and the absorbance of the tag line is scaled to that concentration. This absorbance and the diameter of the gas plume determine the radiance of the plume which, combined with the spectroradiometer's sensitivity, is a relative measure of the probability of detection in open path monitoring. With this information, the AOTF-based spectroradiometer can be designed for maximum impact on satisfying the program goal.

1.2 COMPUTER CODES

Optical spectra are quite complicated, often comprised of several hundred lines of varying strengths and widths, and depend on external factors such as gas pressure, gas temperature, and spectrometer resolution. They also depend on internal factors such as molecular structure, collisional broadening, and Doppler broadening. To handle the spectra of several gases it is essential to utilize computer codes to manipulate the vast amount of data and to analyze the data for key features which

uniquely identify each molecular species. Four key computer codes for spectra manipulation are described here.

1.2.1 QASOFT

A high resolution digitized library of the infrared absorption spectra of gases has been created by Infrared Analysis, Inc. in Anaheim, California. The library includes spectra of more than 180 gases, a complete list is given in Table 1, and most of the spectra are available in resolutions of 0.125, 0.25, 0.5, 1.0, and 2.0 cm^{-1}. We have the library of spectra with resolutions of 0.125 and 1.0 cm^{-1}.

The digitized spectra are provided on 3.5 in. disks in a computer format compatible with the Lab Calc data processing program described next. The digitized spectra are supported by a manual[2] of over 300 pages which presents all the spectra at four different values of resolution and gives commentaries relevant to the quantitative measurement of the gas spectra.

The spectra in the library cover the range from 500 cm^{-1} to 3700 cm^{-1} (except for HF which has a strong band higher than 3700 cm^{-1}). This region is the fundamental infrared region where the rotation and vibration of the molecules absorb radiation efficiently. There is little of value on either side of this region. At higher frequencies there are only overtones which have extremely small absorption coefficients. At lower frequencies there might be good strong rotation lines but because of strong absorption by water vapor they are inaccessible to gases in the open atmosphere.

Most of the spectra were recorded with a resolution of 0.125 cm^{-1} on an Analect RFX-65 Fourier transform spectrometer equipped with a HgCdTe detector. Since the full width, half maximum of a single absorption line at normal temperature and pressure is ~0.2 cm^{-1}, the spectral details are well reproduced. Some of the spectra -- usually of heavy molecules that do not have spectral fine structure -- were recorded with a resolution of 0.5 cm^{-1} on a Digilab FTS-40 spectrometer.

The appearance of a spectrum (line intensity and broadening) is affected dramatically with pressure. To obtain accurate absorption values, the total pressure and gas temperature were kept as close as possible to the conditions encountered in the open atmosphere, i.e., 1 atmosphere and 70 F. These conditions were met by adding just enough of each trace gas to give an absorbance near 0.1 in one atmosphere of nitrogen or oxygen at 70 F. For most gases, the accuracy of the absorption coefficient and of the concentration-pathlength product is thought to be around 5%.[3]

Included with the QASOFT digitized reference library is the **PROCESS** program which generates low-resolution, namely 0.25, 0.50, 1, 2, or 4 cm^{-1}, spectra from the 0.125 cm^{-1} database. It also generates spectra at values of the concentration-path length, i.e., the ppm-m, different from those at which the spectra were measured, although the new ppm-m values should generally be no greater or less than a factor of eight from the experimental values. The program performs the proper scaling, smoothing, shifting, and interpolation necessary to accurately portray the spectral features of infrared

gas spectra as they would appear under actual instrument conditions at the different resolutions and concentration values.

Table 1. The 180 gases in the Digitized Spectra Reference Library.

Hydrocarbons, C1-C5	
Acetylene	Methane
1,3 Butadiene	2-Methyl butane
n-Butane	2-Methyl-2-butene
Cyclo pentene	3-Methyl-1-butene
Cyclopropane	n-Pentane
Ethane	1-Pentene
Ethylene	2-Pentene
Isobutane	Propane
Isobutylene	Propylene
Isoprene	
Non-Aromatic Hydrocarbons, C6 & Up	
Alpha-Pinene	2-Methyl pentane
Beta-Pinene	3-Methyl pentane
Cyclo hexane	2-Methyl-1-pentene
Cyclo hexene	2-Methyl-2-pentene
n-Heptane	4-Methyl-1-pentene
n-Hexane	n-Octane
Aromatic Hydrocarbons	
Benzene	Tertiary butyl benzene
Ethyl benzene	Toluene
Isopropyl benzene	1,2,4 Trimethyl benzene
Mesitylene	0-Xylene
n-Propyl benzene	m-Xylene
Styrene	p-Xylene
Hydrides	
Ammonia	Hydrogen fluoride
Arsine	Hydrogen iodide
Hydrazine	Phosphine
Hydrogen bromide	Water
Hydrogen chloride	
Oxides and Peroxides	
Carbon dioxide	Hydrogen peroxide
Carbon monoxide	Ozone
Ethylene oxide	Propylene oxide
Furan	Tetrahydrofuran
Organic Acids	
Acetic acid, mostly monomer	Formic acid, monomer
Acetic acid, monomer & dimer	Propionic acid, mostly monomer
Acrylic acid, mostly monomer	Propionic acid, monomer & dimer
Acrylic acid, monomer & dimer	
Aldehydes	
Acetaldehyde	Crotonaldehyde
Acrolein	Formaldehyde
Benzaldehyde	Propionaldehyde
n-Butyraldehyde	
Ketones	
Acetone	Methyl isobutyl ketone
2-Butanone	Methyl vinyl ketone
Di-ethyl ketone	
Alcohols	

- Allyl alcohol
- n-Butyl alcohol
- Ethanol
- Isobutanol
- Isopropanol
- Methanol

Esters

- n-Butyl acetate
- Ethyl acetate
- Ethyl acrylate
- Ethyl butyrate
- Ethyl formate
- Methyl acetate
- Methyl acrylate
- Methyl formate
- Methyl methacrylate
- n-Propyl acetate
- Vinyl acetate

Ethers

- Di-ethyl ether
- Di-isopropyl ether
- Di-methyl ether
- Ethyl vinyl ether
- Methyl vinyl ether

Inorganic Nitrogen Molecules

- Dinitrogen pentoxide
- Hydrogen cyanide
- Nitric acid
- Nitric oxide
- Nitrogen dioxide
- Nitrogen dioxide & tetroxide
- Nitrous acid
- Nitrous oxide

Organic Nitrogen Molecules

- Aceto nitrile
- Acrylo nitrile
- Diethyl amine
- 1,1 Dimethyl hydrazine
- Methyl amine
- Methyl nitrite
- Nitro benzene
- Nitro ethane
- Nitro methane
- Nitroso benzene
- Peroxy acetyl nitrate

Sulfur-Containing Molecules

- Carbon disulfide
- Carbonyl sulfide
- Dimethyl sulfide
- Hydrogen sulfide
- Methyl mercaptan
- Sulfur dioxide
- Sulfur hexafluoride
- Tetrahydrothiophene
- Thiophene

Halogenated Methanes

- Bromochloromethane
- Bromoform
- Bromo methane
- Carbon tetrachloride
- Chloro difluoro methane
- Chloroform
- Chloro methane
- Chloro trifluoro methane
- Dichloro difluoro methane
- Dichloro methane
- Dibromomethane
- Iodo methane
- Tetrafluoro methane
- Trichoro fluoro methane

Halogenated Ethanes

- 1-chloro-1, 1 difluoro ethane
- Chloro ethane
- 1,2 Dibromo ethane
- 1,1 Dichloro ethane
- 1,2 Dichloro ethane
- 1,1 Dichloro-1-fluoro ethane
- Trichlorotrifluoroethane
- 1,2 Dichloro tetrafluoro ethane
- 1,1,1,2 Tetrachloroethane
- 1,1,2,2 Tetrachloroethane
- 1,1,1 Trichloro ethane
- 1,1,2 Trichloro ethane

Halogenated Ethenes

- Chloro trifluoro ethylene
- cis-1,2 Dichloroethylene
- Tetrachloro ethylene
- Trichloro ethylene
- Vinyl chloride
- Vinylidene chloride

Halogenated Benzenes

- Bromobenzene
- m-Dichloro benzene

Chloro benzene
2-Chlorotoluene
4-Chlorotoluene
o-Dichloro benzene
p-Dichloro benzene
Fluoro benzene

Miscellaneous

Acetyl chloride
Boron trichloride
Carbonyl fluoride
1,2 Dichloropropane
1,3 Dichloropropane
Exxon 87 gasoline
K-1 Kerosene
Perfluoro butane
Phosgene
Phosphorus trichloride
Silicon tetrafluoride
1,2,3 Trichloropropane

1.2.2 Lab Calc

Lab Calc is a spectra manipulation program from Galactic Industries Corp. in Salem, New Hampshire. The program has several features, some of which are:

- Extensive data processing capabilities
- Comprehensive peak editing and area calculation
- Convenient import and export of spectroscopic data
- Up to 30 levels of contour lines in eight colors
- Three-dimensional graphic capabilities
- What-you-see-is-what-you-get plotting
- Fast display zooming capabilities

Additional programs which extend the data processing capability with some sophisticated quantitative analysis capabilities such as Partial Least Squares[4] are available but were not purchased since their applicability to AOTF-based spectroradiometers is not apparent.

This program can analyze overlapping spectral bands as a sum of fully-resolved ideal peaks. Peaks can be modeled as Gaussian, Lorentzian, or mixed Gaussian-Lorentzian. The modeled peaks are adjusted for the best fit with the Levenberg-Marquardt algorithm.[5] A tabular report of the peak deconvolution analysis gives the center wavelength, width, height, and area of each peak.

Baselines are adjustable with operator-selected approaches which vary from simple two-point linear baselines to sixth-order polynominal curves. Alternatively, the baseline can be adjusted automatically by the program which eliminates the need to preprocess most data. Savitsky-Golay[6] smoothing is available to reduce the effect of noise spikes and to provide spectral derivatives.

When mixtures are encountered, pure spectra of the individual components can be subtracted from the mixture spectra, thereby yielding the underlying peaks and simplifying the identification of the individual components. In this subtraction mode, the concentration-path lengths of the individual components are adjusted to give the best fit to the mixture spectra.

Lab Calc and Process are both written in the Array Basic programming language which is a highly optimized, extremely fast array-oriented language which is integrated with and takes advantage of the display graphic environment. The language includes almost 200 Statements and Functions. The array sizes are limited only by computer memory; the Lotus/Intel expanded memory standard is used to make megabytes of memory available for data manipulation. Typical timings on an AT with a 6 MHz coprocessor are:

- 4 seconds to invert a 30 x 30 matrix of random numbers
- 2 seconds to multiply two 32 k point arrays
- 2 seconds to convert 8,000 point spectrum from transmission to absorbance

This language, as well as the source program, is provided with Lab Calc.

1.2.3 GRAMS/386

GRAMS/386 is the new spectra manipulation program from Galactic Industries Corp. It provides all the features of **Lab Calc** under the friendly Microsoft Windows graphical user interface. This totally new product is a true 32 bit program which takes full advantage of 80386 and 80486 processors. For computationally intensive applications **GRAMS/386** runs from two to ten times faster than **Lab Calc**. In addition **GRAMS/386** incorporates an innovative hierarchical, relational database designed to efficiently manage the huge quantities of raw data generated in spectroscopic measurements.

GRAMS/386 includes new documentation, improved menu dialogs, and a friendlier user interface. The use of Windows Dynamic Data Exchange (DDE) and Galactic's Array Basic Control Labuage (ABC) simplify interfacing with instrumentation. Array Basic application programs such as curvefit, spectra subtraction, and baseline corrections have been improved. Furthermore, peak marks are placed so that they do not overlap and connecting lines are given that indicate each peak. Font colors of the lines and labels are automatically chosen for maximum contrast with the trace box color.

GRAMS/386 is a new generation product which largely has backward compatibility to **Lab Calc**. However, **GRAMS/386** uses an enhanced file format that is not compatible with **Lab Calc**. This incompatibility is the reason that **Lab Calc** was used for all the results given here since, at the time they were obtained, the QASOFT Atlas of spectra existed only in the old format. This limitation is being removed with the eminent release of a **GRAMS/386**-compatible QASOFT Atlas of spectra.

1.2.4 PEAKTB

The Peaks Table given by **Lab Calc** is ordered by wavelength and includes some peaks which are obviously not true peaks, e.g., negative peaks which result from noise or peaks with negative areas due to incorrect baseline determination. To obtain more useful tables of spectral peaks, a Fortran77 program, PEAKTB, was written to read the **Lab Calc** generated table and generate two new tables.

The first table, called the Modified Peaks Table, is formed by eliminating all peaks with absorbances less than an operator-specified value and all peaks with absorbances above another operator-specified value (high absorbance values[7] occasionally occur at the very ends of the wavelength range being measured and result from instrumention error). This table is still ordered from large to small wavelengths and is simply a cleaner version of the original Peaks Table.

The second table, called the Sorted Peaks Table, is formed by using the straight insertion technique to order the first table from the highest to the lowest absorbance value. Although straight insertion is an N^2 routine for N elements, and nominally should be used for small N, say $N < 50$, the program runs very fast on a 386 computer and there is no apparent penalty for using this "slow" algorithm.

The Modified Peaks Table is most useful for locating atmospheric interferences to an absorption line of a gas of interest. The Sorted Peaks Table is most useful for finding the highest absorbance lines for a gas of interest, i.e., those lines most useful for high sensitivity. Both tables contain:

- Peak Number
- Peak Absorbance
- Wavelength of Peak in μm
- Left Edge in cm-1
- Peak Location in cm-1
- Right Edge in cm-1
- Line Width in cm-1
- Line Area in cm-1

Furthermore, both tables can be linearly scaled to any concentration-pathlength product.

1.3 ABSORPTION MEASUREMENTS

1.3.1 Active Measurements

In active measurement, a hot source is used such as a SiC glower is used for identification and quantification of gases in the atmosphere. The radiance of the source is determined by the temperature of the SiC rod. The temperature of the source is held around 1550 K and considered to be a blackbody radiator. A bistatic configuration is used in which the radiation source and detector are at different ends. The airborne effluents are detected and analyzed during the crossing of the optical path of the instrument. The radiation intensity attenuated by the effluent plume is determined by Beer's law and given by the equation

$$I(\upsilon) = I_o(T_s, \upsilon)e^{\sum_1^n [-a(\upsilon)CL]} \qquad (1)$$

where $I_0(T_S,\upsilon)$ is the background radiation calculated with the Planck function evaluated at the source temperature, T_S, $\alpha(\upsilon)$ is the absorptivity of the i^{th} component, C is the concentration of the i^{th} component and L is the pathlength. This equation does not take into account other possible participants such as plume emission, attenuation and emission by the atmosphere, scattering and reflection of radiation by other sources besides the background and the plume. The absorbance calculated from the Beer's law is given by the equation

$$Abs = -\log\left(\frac{I(\upsilon)}{I_o(\upsilon)}\right) = a(\upsilon)CL. \qquad (2)$$

Other factors such as atmospheric pressure and resolution of the instrument have not been added to the equation but are expected to affect the linearity of the Beer's law.

1.3.2 Passive Measurements

In many cases, hot sources such as the SiC glower cannot be used for the detection and characterization of effluents in a plume. Passive measurements become the only alternative in order to gain an insight of the chemical composition. Passive measurements are made against a background which, in general, has a similar temperature to the plume. Under these conditions, detection and quantification of the effluents is difficult. Beer's law does not provides an accurate representation of the concentration - pathlength product. The net radiation from the effluents in the plume in power per unit area per steradian per wavenumber is given by

$$I(\upsilon) = I_o(T_s, \upsilon)e^{\sum_i^n [-a(\upsilon)CL]_i} + I_a(T_a, \upsilon)[1 - e^{\sum_i^n -a(\upsilon)CL]_i}] \qquad (3)$$

where I_a is the Plank function evaluated at the effluent plume temperature, T_a. The absorbance from this equation is given by:

$$Abs = -\ln[\frac{I - I_a}{I_o - I_a}]. \qquad (4)$$

1.4 ATMOSPHERIC EFFECTS

1.4.1 Temporal Effects

There are three basic temporal frames for atmospheric effects.[8] Short time effects are caused by the wind moving small-scale refractive index inhomogeneities through the observation path. The effect is a 20% fluctuation in the intensity which increases at humidities over 70%.[9] The scintillation frequency is given by

$$f = (2L)^{-1/2} v_w \qquad (5)$$

where is the wavelength, L is the observational path length, and v_w is the wind velocity orthogonal to the line of sight. The fluctuation amplitude can be reduced, i.e., averaged out, with radiation collecting apertures larger than $(L)^{1/2}$, e.g., for apertures larger than 20.5 cm for 14 μm radiation over a 3 km path length. Furthermore, the atmosphere is essentially "frozen" by taking measurements over short time periods, on the order of 10 ms or less.

The medium time effect is beam wander caused by large blobs of perturbed refractive index moving through the line of sight. The angular deviation is roughly independent of wavelength but is

proportional to $L^{1/2}$: over a 3 km path length, the beam wander is 8 μrad. The frequency of this disturbance is on the order of 1 Hz. Fortunately, beam wander does affect sensitivity and is too small to significantly affect plume location.

The long time effect is simply due to the atmosphere not being a homogeneous gas. For times longer than 30 seconds, atmospheric constituents at a particular location change due to wind, turbulence, convection, and/or diffusion. This effect can be an advantage by moving distant trace gases of interest into the spectroradiometer field of view.

There is one more temporal effect: the limitation on improving accuracy by averaging many measurements. If the individual measurements are independent, the signals will add directly but the uncorrelated noise will add only as a root mean square, thereby improving the signal-to-noise ratio. However, temporally spaced measurements of the atmosphere are not necessarily independent. Recent measurements are inconclusive in that published Lidar (Light detection and ranging) measurements show a temporal correlation for 100 seconds which limits the improvement obtainable by this technique to about 5-fold, with little improvement obtained by averaging more than 100 measurements.[10] In contrast, recent measurements at the Los Alamos National Laboratory with their Lidar system show no evidence of temporal correlation.[11]

1.4.2 Absorption Effects

There are two general types of absorption: continuum and line. The largest continuum absorption is from water vapor in the 7 to 30 μm region. The continuum arises from mixtures of monomers and dimers, and is the result of overlapping wings of many broad lines whose centers are outside the continuum region.[12] Line absorption causes spectral interference when absorption lines of one gas masks an absorption line of a trace gas. It is a serious problem which has not been completely solved. Present technology can identify up to 10 thoroughly mixed minority species.

These absorptions limit the measurement range for trace gases and restrict the most useful infrared regions to the nine transmission windows in Table 2, where window IX is only partially transmitting.[1,13]

Table 2. The nine infrared atmospheric transmission windows through which long-path monitors must operate.

Window	Wavelengths μm	Window	Wavelengths μm
I	0.70 - 0.92	VI	2.9 - 4.2
II	0.92 - 1.1	VII	4.5 - 5.3
III	1.1 - 1.4	VIII	7.5 - 13.8
IV	1.4 - 1.8	IX	15.8 - 22.2
V	1.9 - 2.6		

The origin of these atmospheric transmission windows lies in the absorption characteristics of the three most common infrared-absorbing atmospheric gases.[1] These gases and their nominal concentrations are given in Table 3. Their spectra obtained from the Hanst library are shown in Figure 1. During experimental measurements, Beer's law is obeyed at concentration-pathlength products leading to a maximum absorbance of 0.1 to 0.2. Therefore, their atmospheric absorbances must be scaled to the value corresponding to their atmospheric concentration.

Table 3. Five normal atmospheric constituents cause virtually all atmospheric absorption effects.

Chemical Name	Formula	Concentration, ppm
Water	H_2O	15,000
Carbon dioxide	CO_2	360
Methane	CH_4	1.7
Nitrous oxide	N_2O	0.3
Carbon monoxide	CO	0.2

The other two major atmospheric constituents, nitrous oxide and carbon monoxide, must also be considered since their atmospheric concentrations occasionally mask trace gases by spectroscopic interference. All other gases have such low concentrations, < 27 ppb,[14] that they need not be considered except in special cases of spectral interference.

[1] O_2 and N_2 have high concentrations but extremely weak infrared absorption since they are homonuclear diatomic molecules.

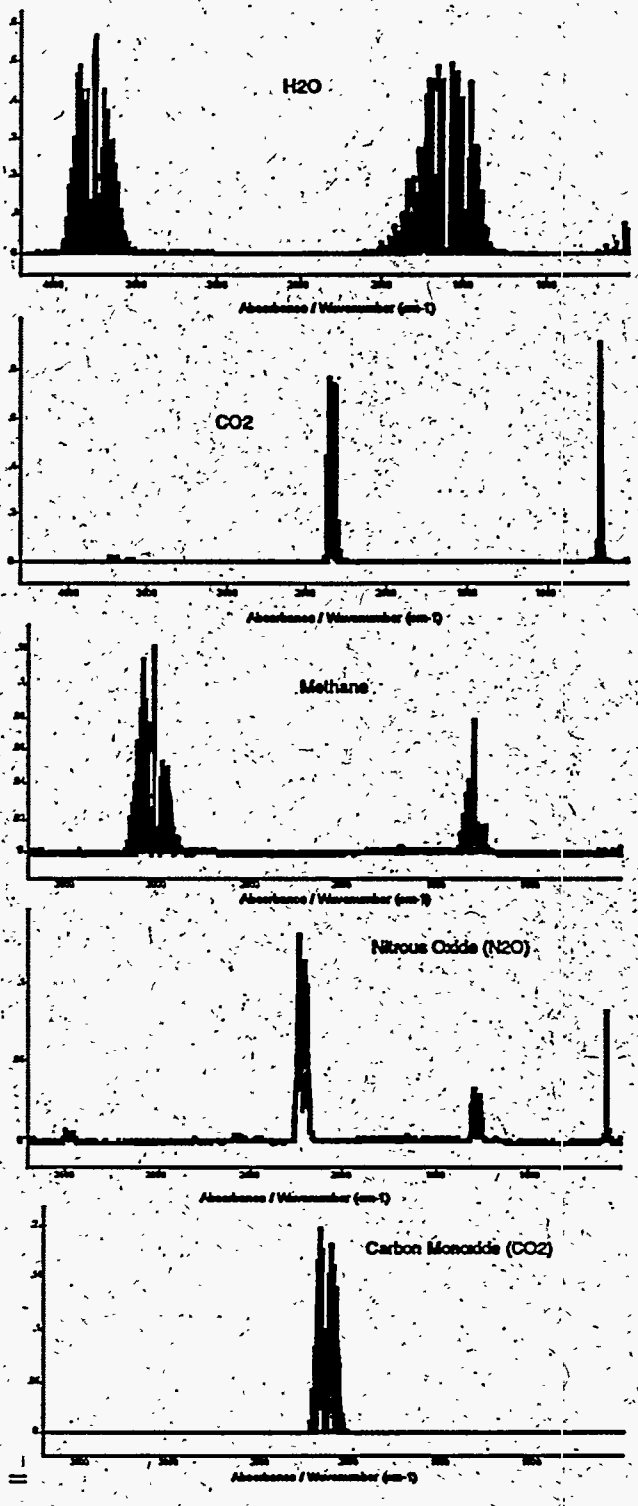

Figure 1 — These five atmospheric spectra determine the transmission windows and most of the spectra interferences.

1.5 SOURCE GASES

In a simulated gas release, several infrared-emitting air toxic evaporation rates were measured at the Savannah River Site (SRS) and given in Table 4. A list of 42 gases is given in Table 5. The Chemical Abstract Service (CAS) Registry Numbers are from P. H. Howard and M. Neal.[15] The preferred name, from the same reference, is given with an occasional second name in parentheses, except for sulfamate which has a long preferred name.

We have three sources for infrared spectra of gas vapors: (1) the 180 gas Digitized Reference Library, (2) spectra measured specifically for this program by Philip Hanst at Infrared Analysis, Inc., and (3) the > 6,500 spectra **Aldrich Library of FT-IR Spectra, Volume 3: Vapor Phase.** Source 2 is used for gases not included in Source 1. These two sources are preferred because the spectra are digitized and provided on computer disks. Source 3 encompasses a large number of gases but does not include any of the 42 gases not available from the first two sources. The spectra source for each gas of interest is included in Table 5.

Of the 42 molecules, we have 31 in the Digitized Reference Library which were measured with resolutions of 0.125 and/or 1.0 cm^{-1}. K-1 kerosene is representing all kerosenes which are actually different mixtures with exact mixture ratios depending on the manufacturer. Eight other gas spectra were measured for us with 0.5 cm^{-1} resolution by P. Hanst, Infrared Analysis Inc.

Of the three gases for which we have no spectra, hydroxylamine nitrate would probably dissociate quickly to HNO_3 and H_3NO, and sulfite rapidly fumes in air to H_2SO_4. Sulfamate, with the complete chemical name of Sulfamic acid, monoammonium salt, must have very low vapor pressure, rapid dissociation, or rapid reaction since we have not been able to obtain data on this gas species. It is unlikely that these three gases would exist in measurable concentrations in expected scenarios. They were therefore eliminated from further consideration.

Table 4. Infrared-emitting air toxics from a simulated release.

Chemical Name	Emission Rate, g/s
Nitric acid	3.570×10^{-0}
Xylene	2.471×10^{-3}
methyl Ethyl ketone (2-Butanone)	9.359×10^{-4}
Toluene	6.301×10^{-4}
Ethylene-glycol	5.835×10^{-4}
Methyl alcohol (Methanol)	4.875×10^{-4}
methyl Isobutyl ketone (4-methyl 2-Pentanone)	3.673×10^{-4}
Hexane	3.310×10^{-4}
Methylene chloride	1.832×10^{-4}
1,1,1-Trichloroethane	6.638×10^{-5}
ethyl Benzene	2.309×10^{-5}
Trichloroethylene	1.587×10^{-5}
Phenol	1.731×10^{-6}
Vinyl acetate	1.442×10^{-6}
Napthalene	7.211×10^{-7}

1.6 INFRARED GAS SPECTRA

1.6.1 Source Gas Spectra in Reference Library

The effect of measuring spectra at different resolutions is illustrated in Figure 2. As the measured spectra is broadened with increasing resolution, the absorbance of an isolated peak much narrower than the resolution is reduced in direct proportion to the resolution. For lines with widths close to the resolution, the absorbance will also decrease with increasing resolution, but slower than linearly. Finally, the absorbance of lines much broader than the resolution are essentially unchanged. A commonly occurring case is a narrow line in close proximity to several other lines. In this situation, increasing the resolution may decrease or increase the absorbance since the increased resolution reduces the narrow line absorbance but encompasses more of the adjacent lines.

Since heavy molecules have primarily broad lines or closely spaced narrow lines, and the optical throughput of a spectroradiometer is inversely proportional to the resolution, 2 cm^{-1} resolution is a reasonable choice. For an AOTF-based spectroradiometer, the time needed to scan a region or band of wavelengths is proportional to the resolution. Again, 2 cm^{-1} is a reasonable compromise between speed and optical throughput versus accuracy, and is the value for most of the spectra given herein.

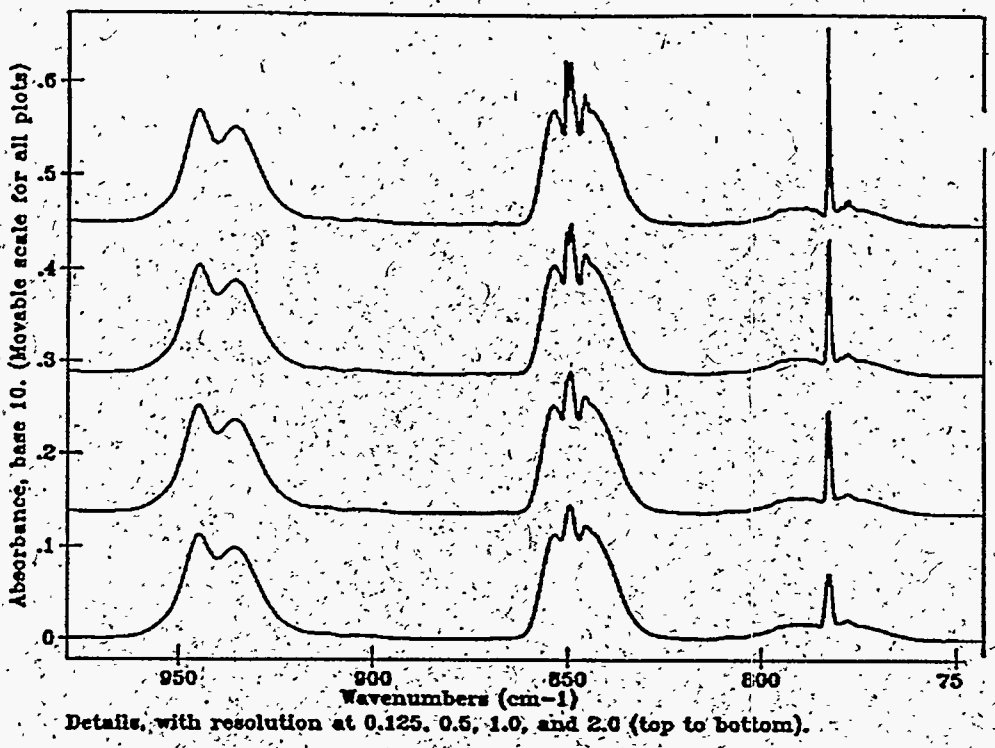

Figure 2— Increasing the resolution decreases the absorbance of narrow lines but has little effect on broad lines or on closely spaced narrow lines as shown by this Trichoroethylene spectra shown, from top to bottom, at resolutions of 0.125, 0.5, 1.0, and 2.0 cm^{-1}.

Of the 31 source gases in the Digitized Reference Library, 29 were measured at 0.125 cm^{-1} resolution and could be properly modified to simulate spectra measurements at 2 cm^{-1} resolution. Two gases, nitrous acid and phosphorous trichloride, were measured at 1.0 cm^{-1} resolution and therefore could not be properly modified to simulate measurements at 2 cm^{-1} resolution. The spectra of these 31 source gases are presented in Figures 3 through 12.

Table 5. Many chemicals are associated with the processing of industrial materials.

CAS	Chemical Name	Formula	Spectra Source
7664-41-7	Ammonia	NH_3	IA Library
71-43-2	Benzene	C_6H_6	IA Library
106-97-8	Butane	C_4H_{10}	IA Library
71-36-3	Butanol (n-Butyl alcohol)	$C_4H_{10}O$	IA Library
78-93-3	2-Butanone	C_4H_8O	IA Library
56-23-5	Carbon tetrachloride	CCl_4	IA Library
75-71-8	Dichlorodifluoromethane (Freon 12)	CCl_2F_2	IA Library
112-40-3	Dodecane	$C_{12}H_{26}$	P. Hanst
110-54-3	Hexane	C_6H_{14}	IA Library
302-01-2	Hydrazine	H_4N_2	IA Library
7647-01-0	Hydrogen chloride	HCl	IA Library
74-90-8	Hydrogen cyanide	HCN	IA Library
7664-39-3	Hydrogen fluoride	HF	IA Library
7722-84-1	Hydrogen peroxide	H_2O_2	IA Library
7783-06-4	Hydrogen sulfide	H_2S	IA Library
13465-08-2	Hydroxylamine nitrate	$H_4N_2O_4$	———
8008-20-6	Kerosene	—	IA Library
74-82-8	Methane	CH_4	IA Library
67-56-1	Methanol	CH_4O	IA Library
7697-37-2	Nitric acid	HNO_3	IA Library
10102-44-0	Nitrogen dioxide	NO_2	IA Library
11104-93-1	Nitrogen oxide	NO	IA Library
10544-72-6	Nitrogen tetroxide (dimer)	N_2O_4	P. Hanst
7782-77-6	Nitrous acid	HNO_2	IA Library
10024-97-2	Nitrous oxide	N_2O	IA Library
64771-72-8	normal petroleum Paraffin (n-Pentane)	C_5H_{12}	IA Library
108-10-1	4-methyl 2-Pentanone	$C_6H_{12}O$	IA Library
107-66-4	dibutyl ester Phosphoric acid	$C_8H_{19}O_4P$	P. Hanst
1623-15-0	monobutyl ester Phosphoric acid	$C_4H_{11}O_4P$	P. Hanst
126-73-8	tributyl ester Phosphoric acid (TBP)	$C_{12}H_{27}O_4P$	P. Hanst
7719-12-2	Phosphorous trichloride	PCl_3	IA Library
10025-87-3	Phosphoryl chloride	$POCl_3$	P. Hanst
7773-06-0	Sulfamate	$H_6SN_2O_3$	———
14265-45-3	Sulfite	SO_3	———
10025-67-9	Sulfur chloride	S_2Cl_2	P. Hanst
7446-09-5	Sulfur dioxide	SO_2	IA Library
7719-09-7	Thionyl chloride	$SOCl_2$	P. Hanst
108-88-3	Toluene	C_7H_8	IA Library
79-01-6	Trichloroethylene	C_2HCl_3	IA Library
108-38-3	m-Xylene	C_8H_{10}	IA Library
95-47-6	o-Xylene	C_8H_{10}	IA Library
106-42-3	p-Xylene	C_8H_{10}	IA Library

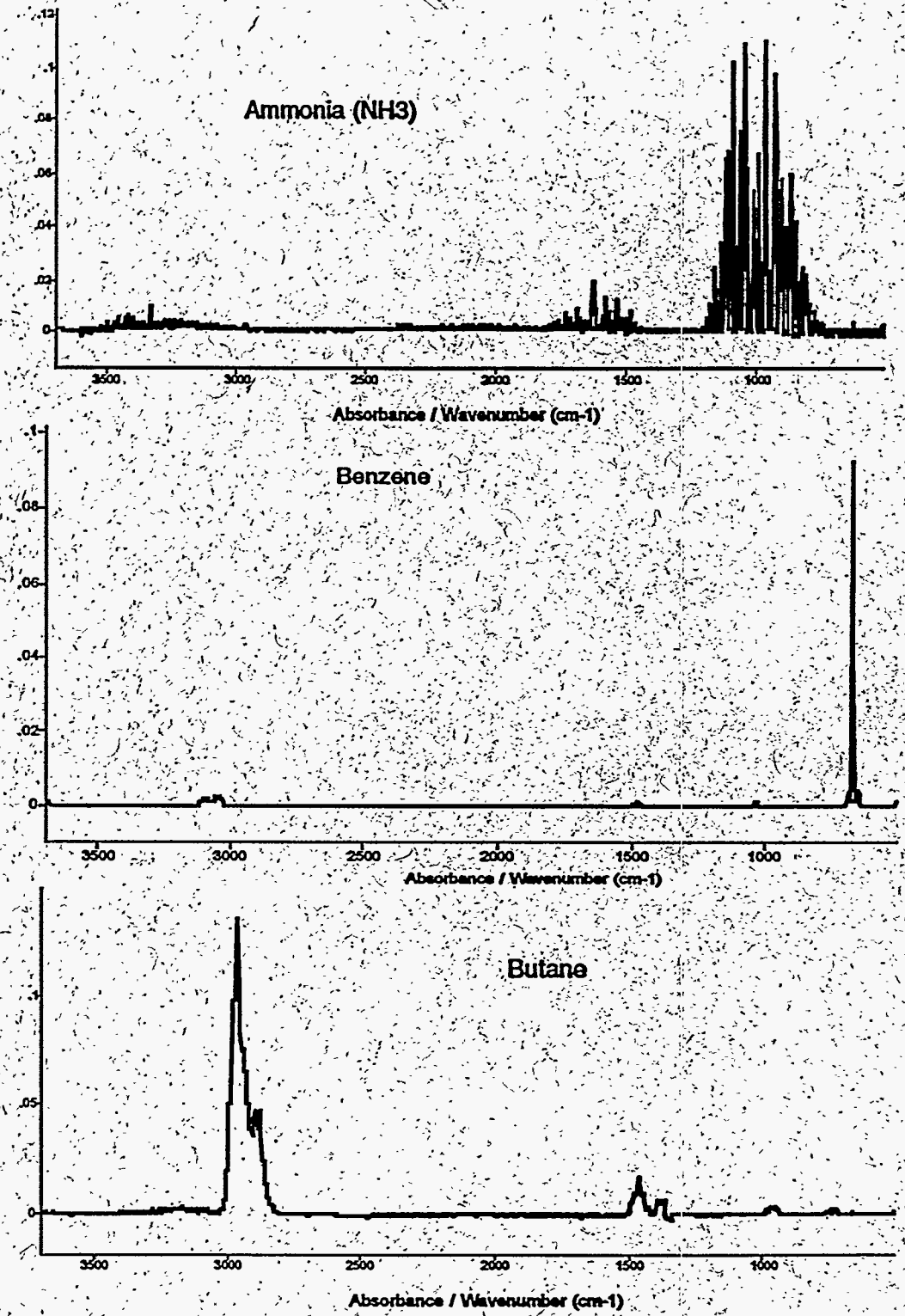

Figure 3 — Spectra of Ammonia (85), Benzene (20), and Butane (151).

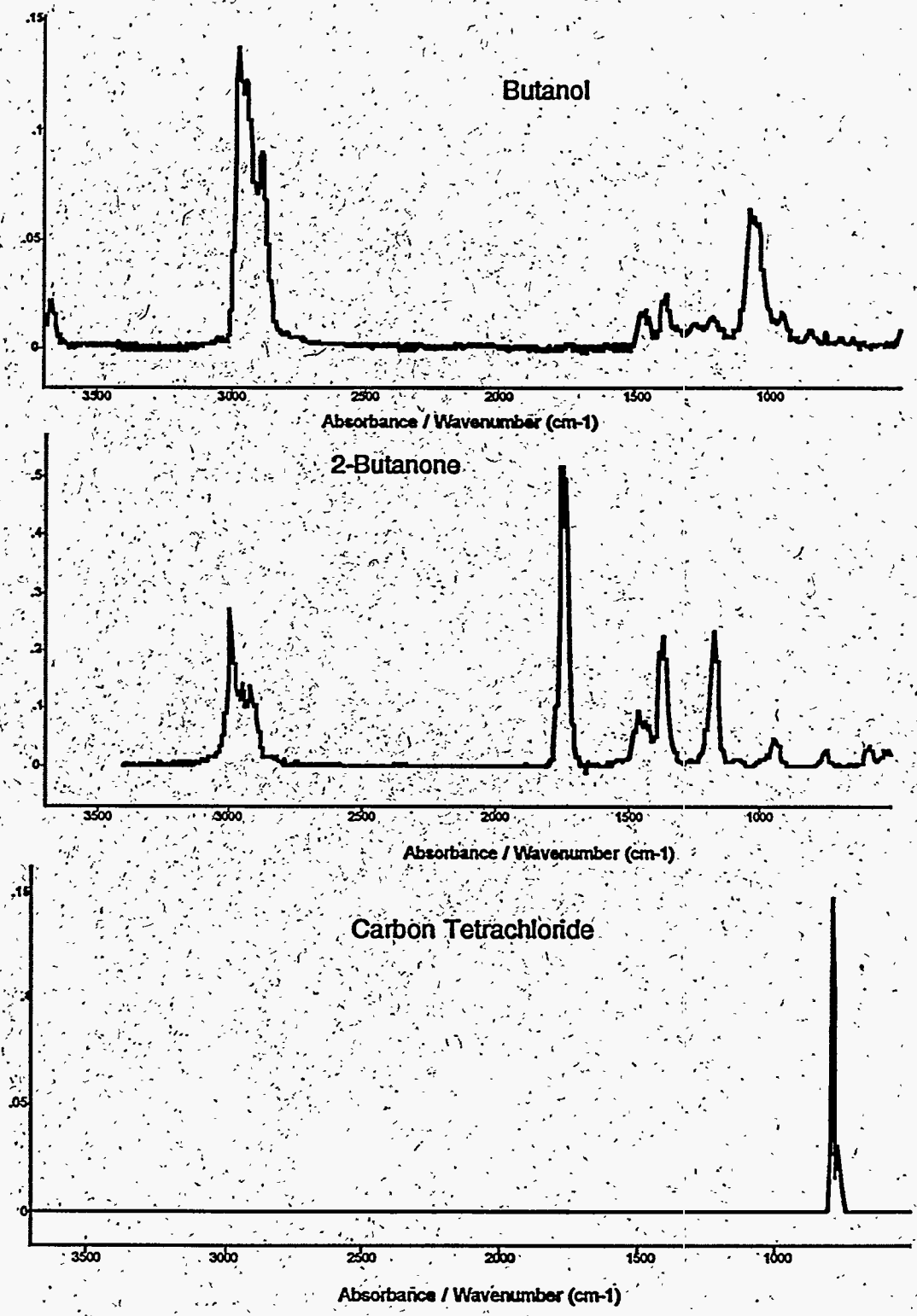

Figure 4 — Spectra of Butanol (300), 2-Butanone (762), and Carbon tetrachloride (27).

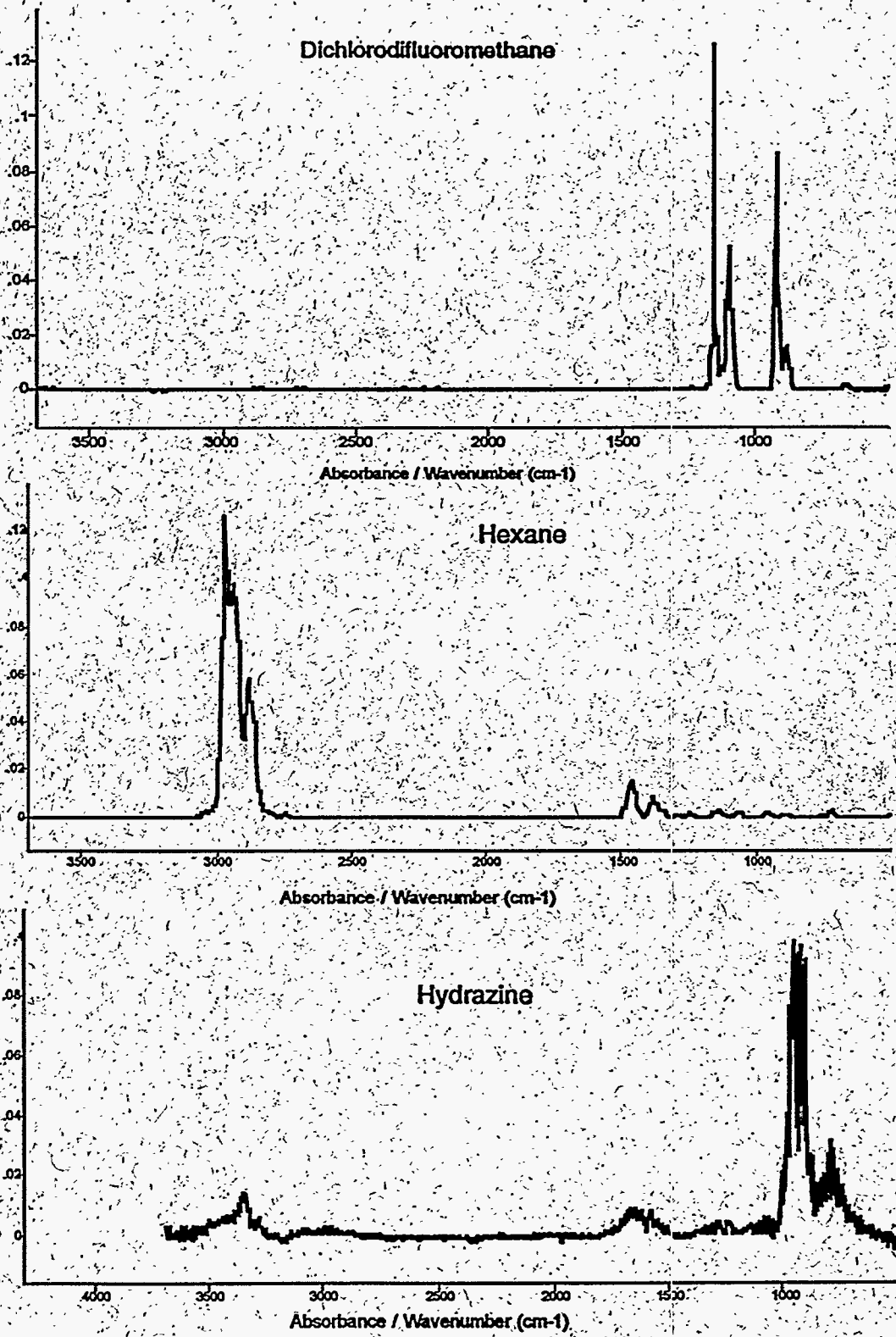

Figure 5 — Spectra of Dichlorodifluoromethane (20), Hexane (121), and Hydrazine (400).

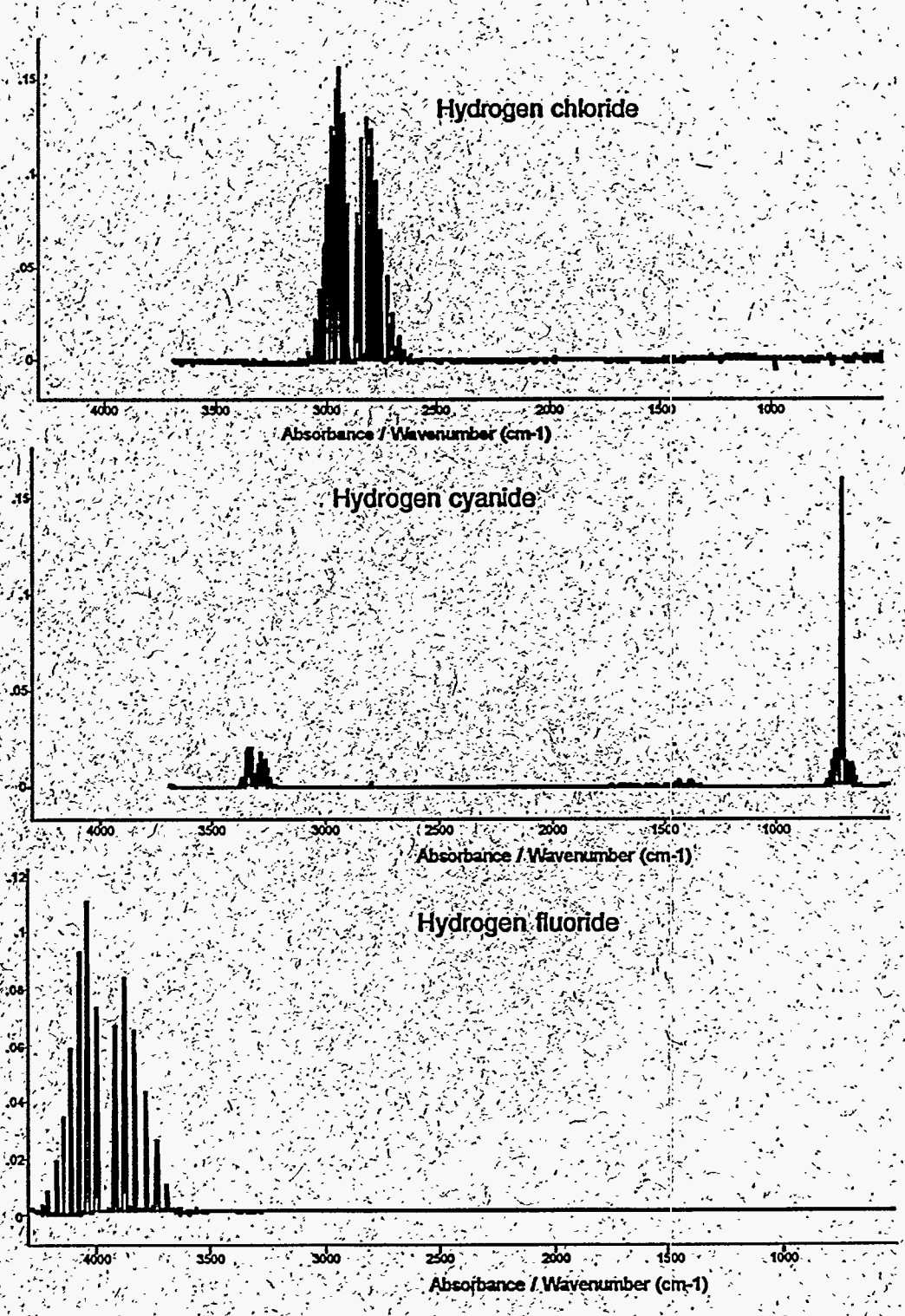

Figure 6 — Spectra of Hydrogen chloride (285), Hydrogen cyanide (36), and Hydrogen fluoride (30).

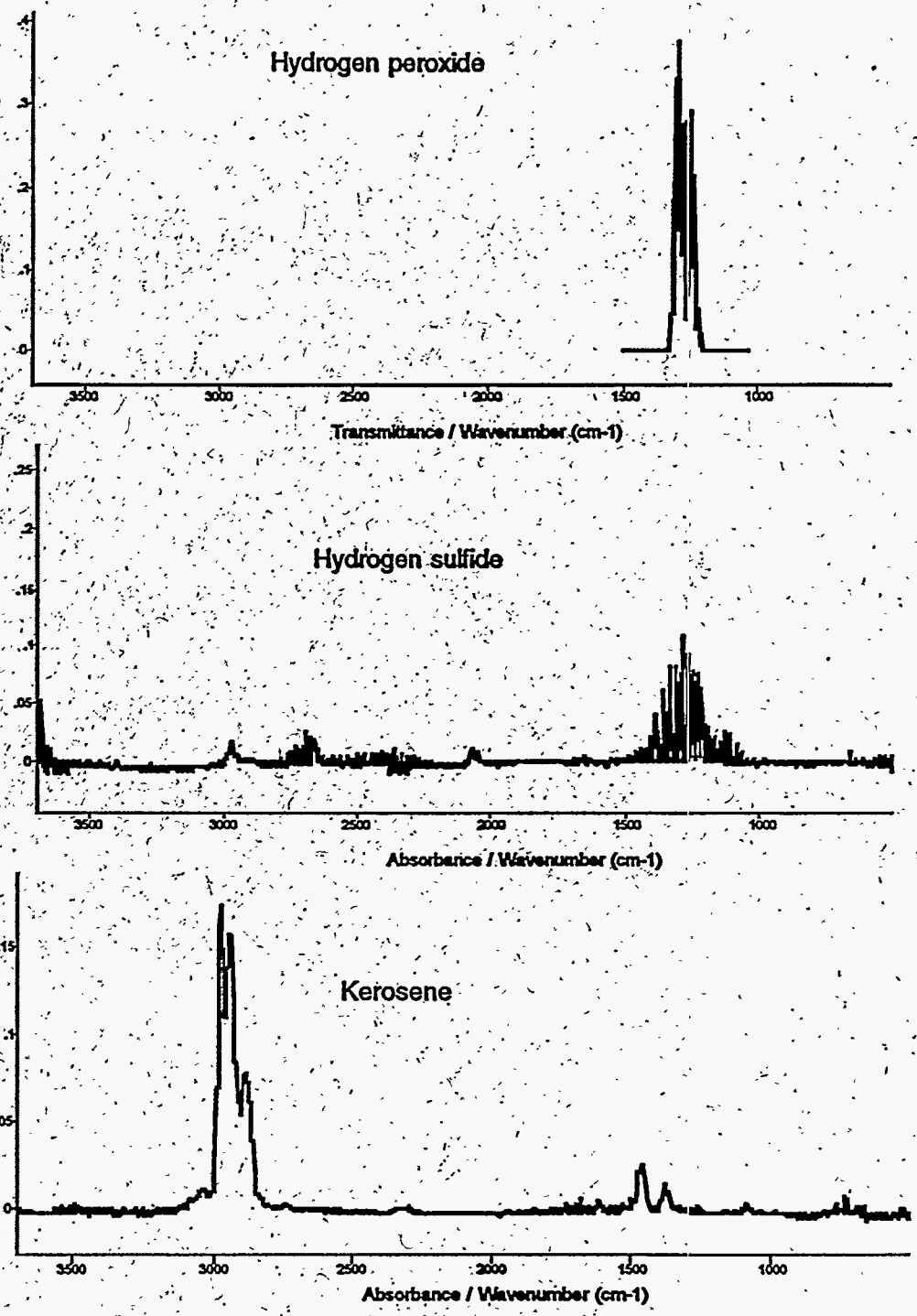

Figure 7 — Spectra Hydrogen peroxide (1000), Hydrogen sulfide (32000), and Kerosene (200).

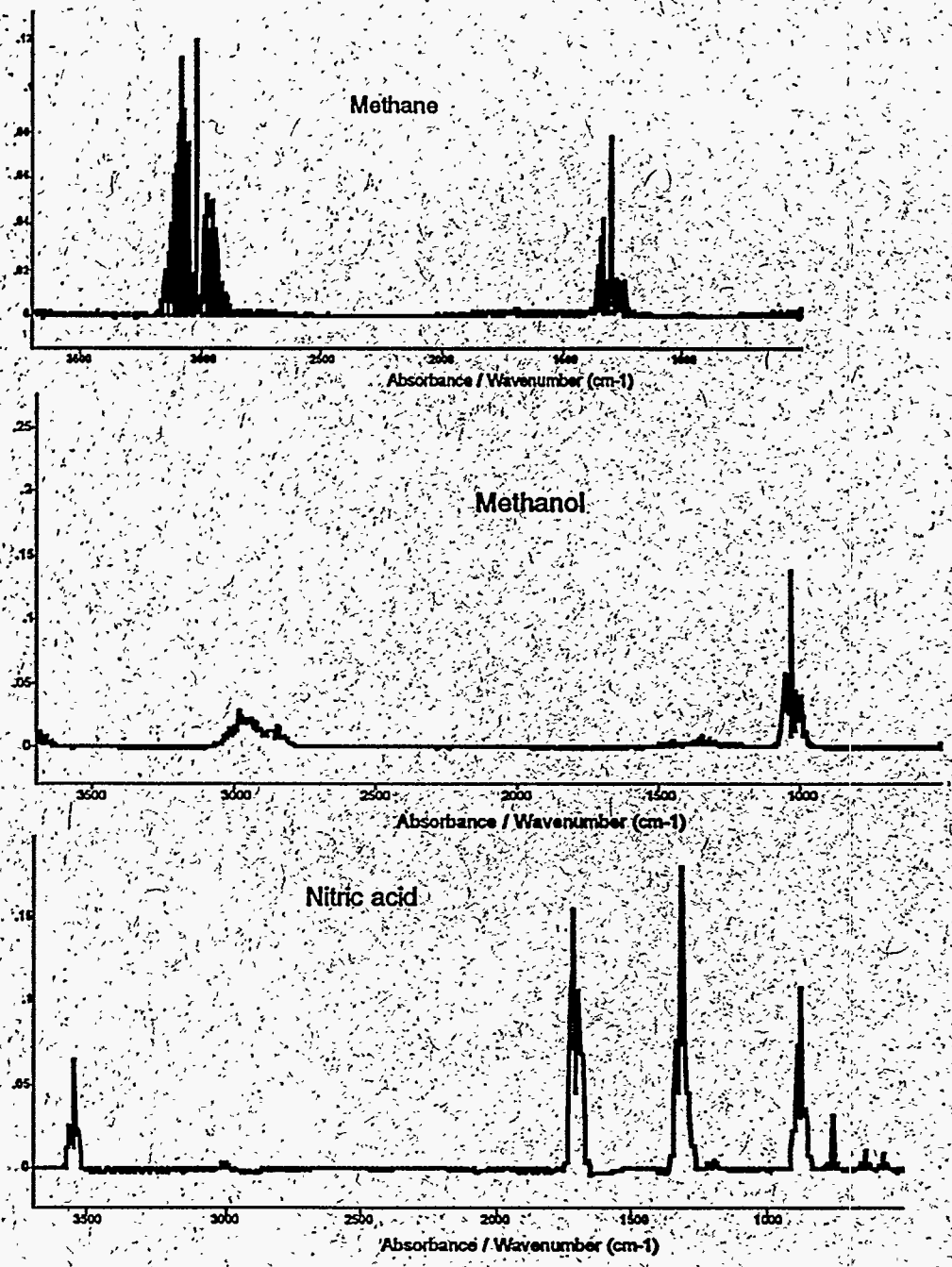

Figure 8 — Spectra of Methane (128), Methanol (141), and Nitric Acid (140).

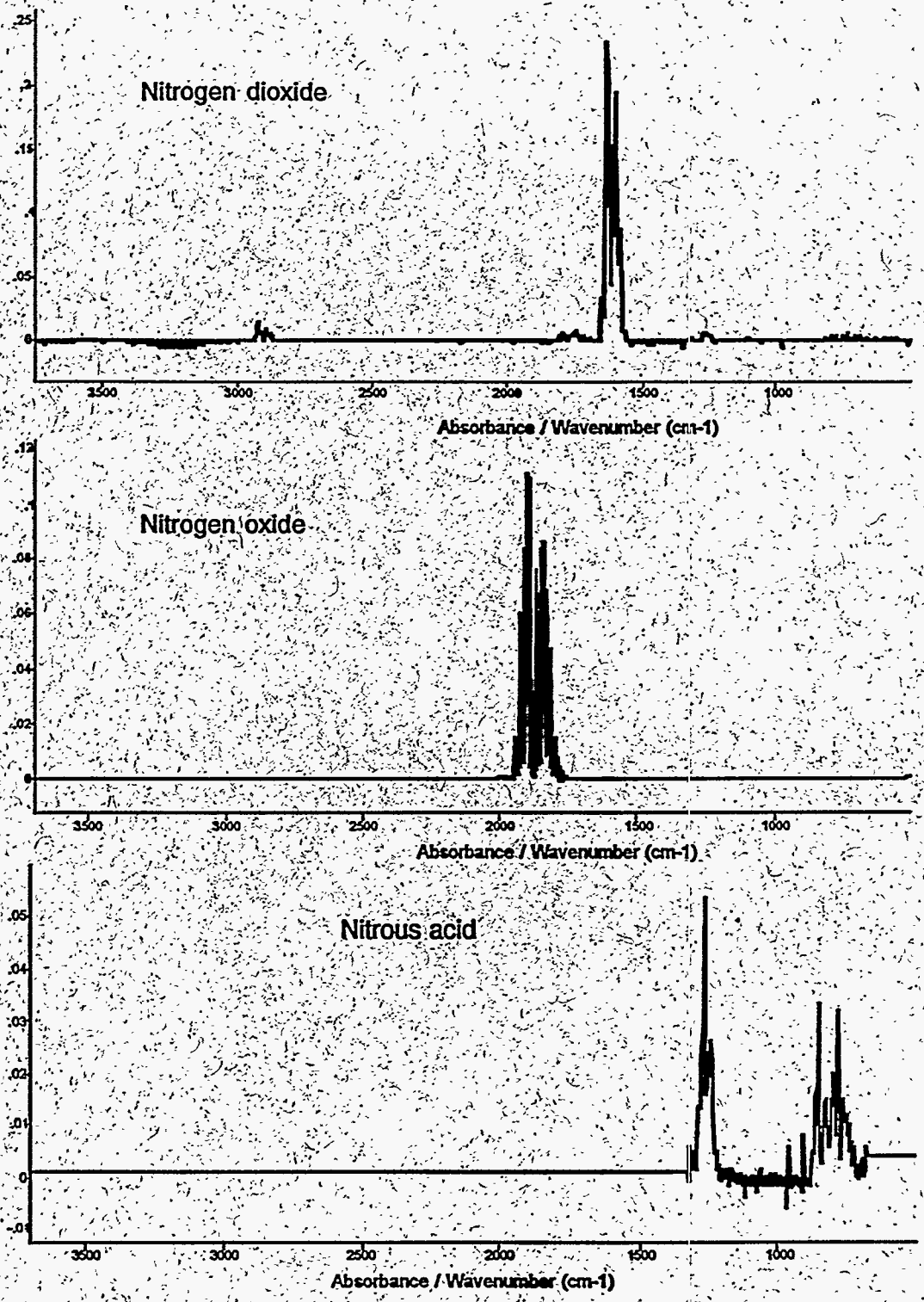

Figure 9 — Spectra of Nitrogen dioxide (125), Nitrogen oxide (625), and Nitrous acid (10).

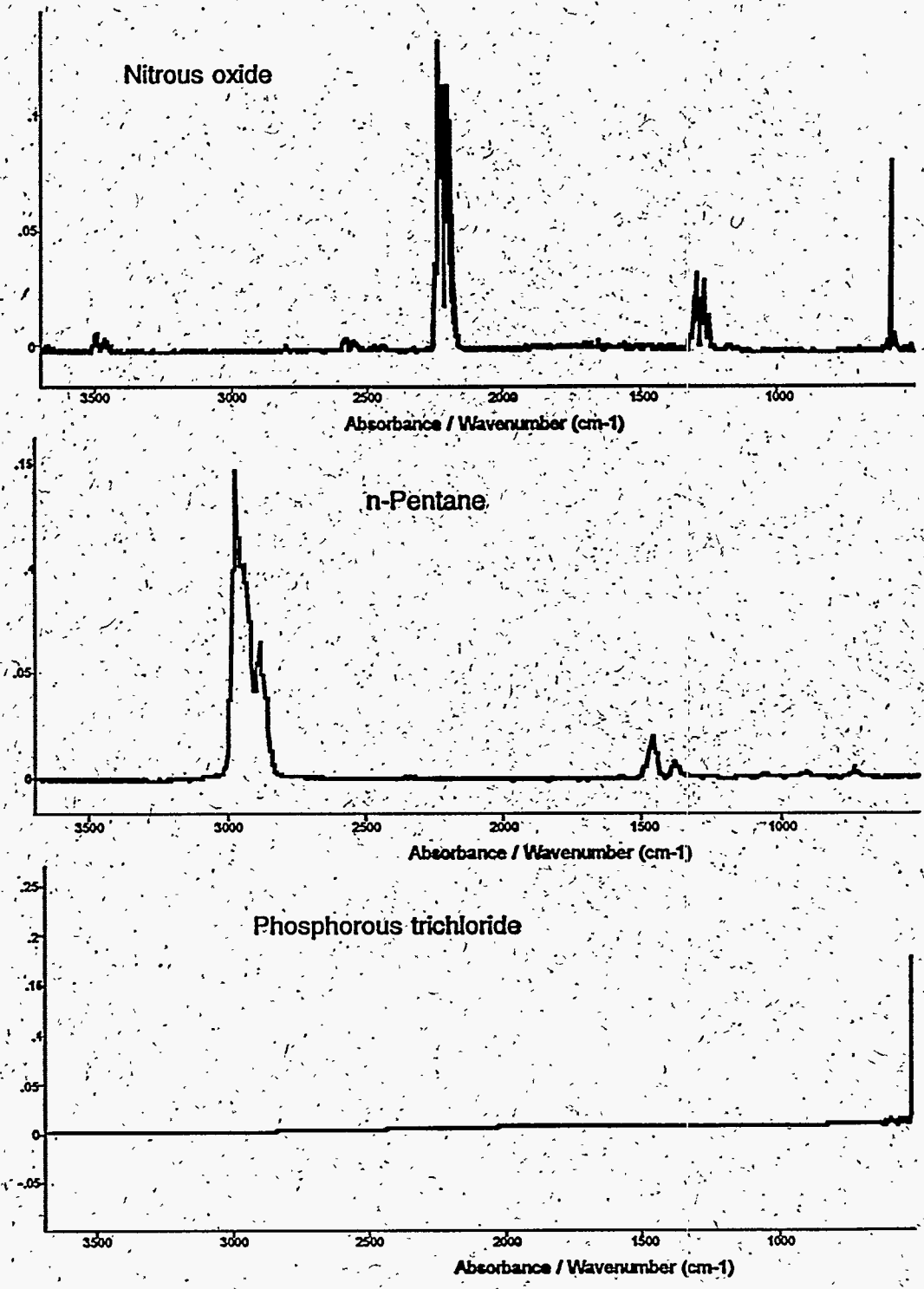

Figure 10 — Spectra of Nitrous oxide (80), n-Pentane (152), and Phosphorous trichloride (700).

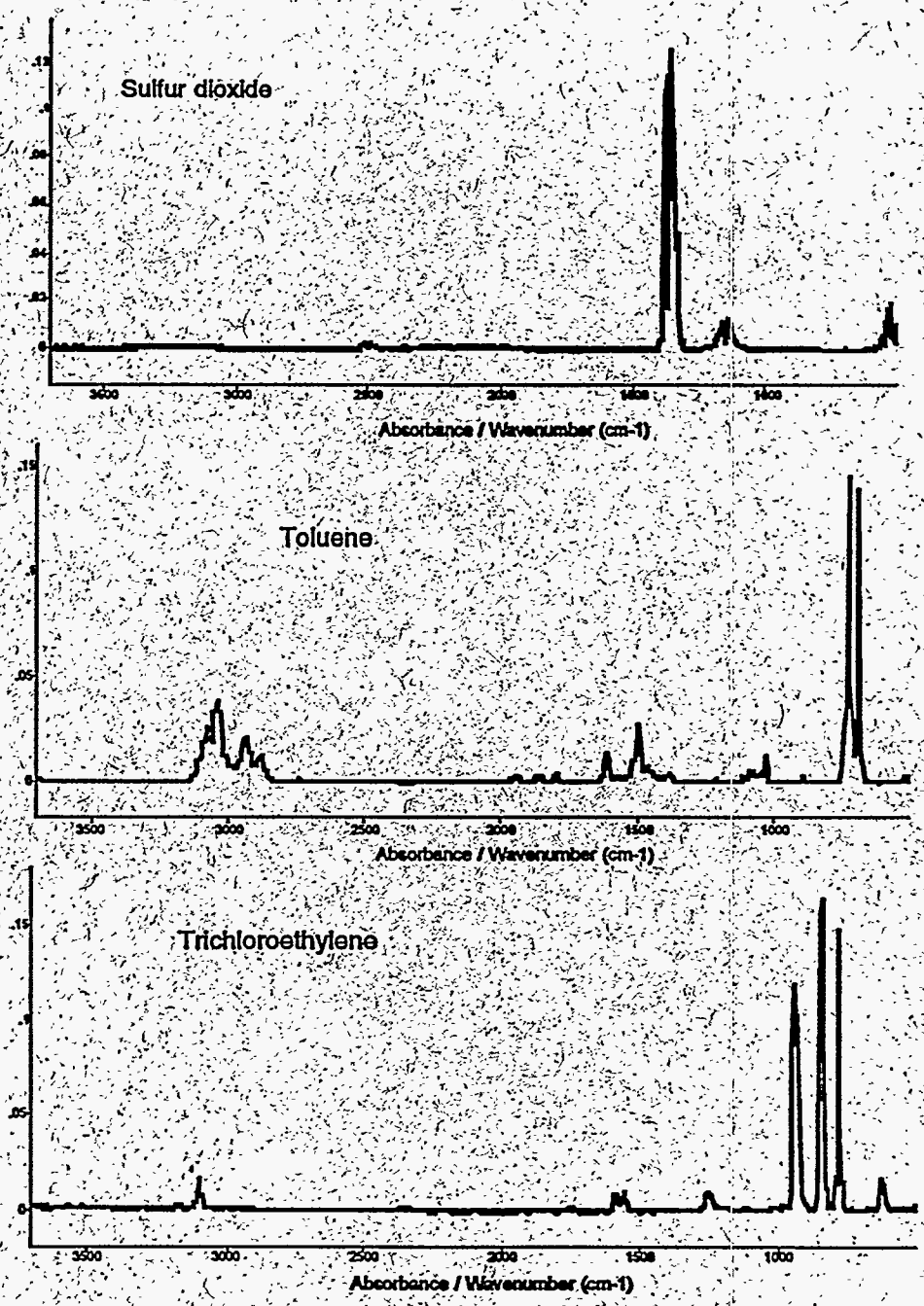

Figure 11 — Spectra of Sulfur dioxide (125), Toluene (137), and Trichloroethylene (160).

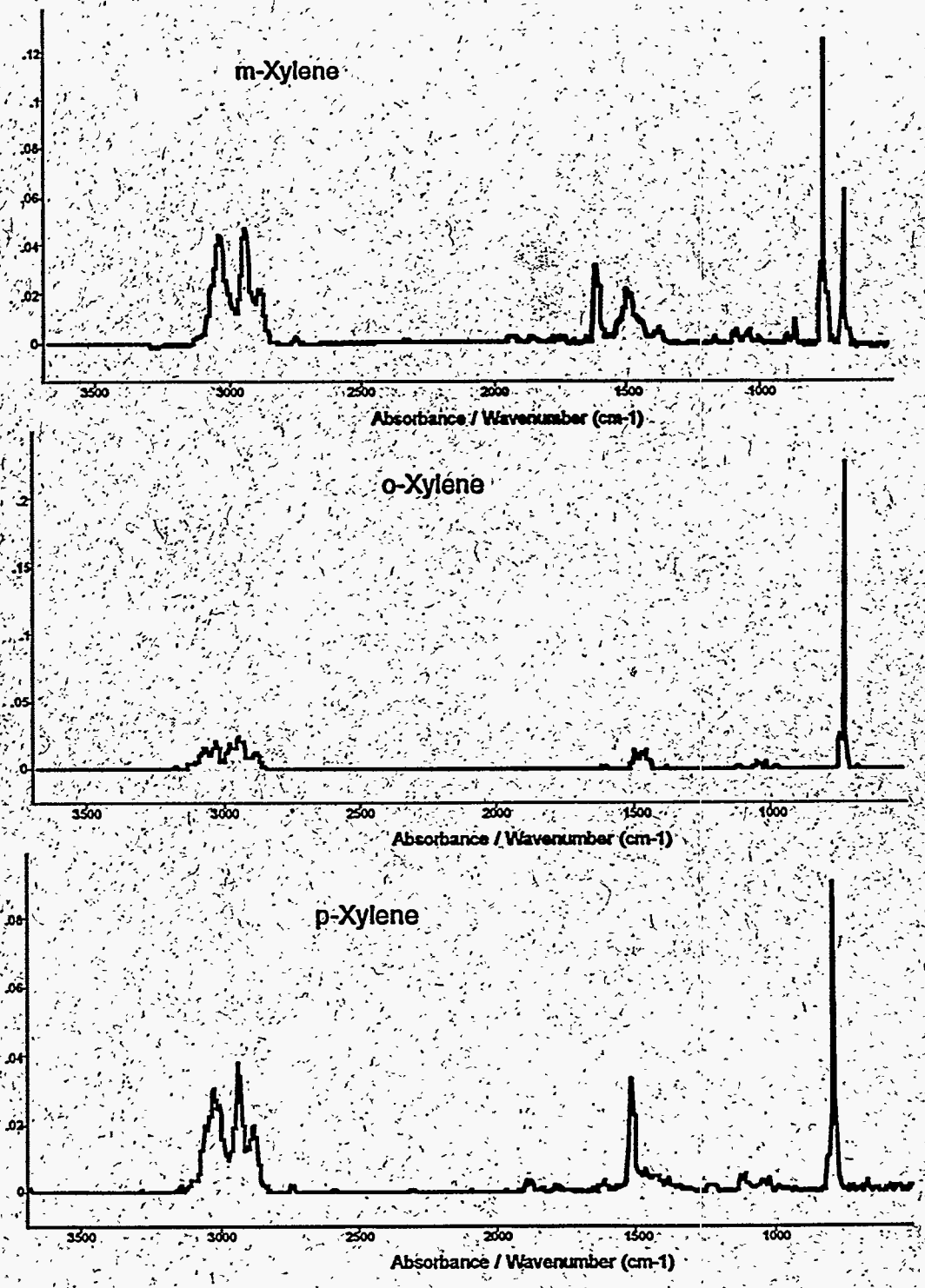

Figure 12 — Spectra of m-Xylene (200), o-Xylene (100), and p-Xylene (200).

These spectra exhibit the major correlations with molecular structure which are generally useful for distinguishing different classes of molecules. Table 6 lists the major spectra-structure correlations for the 2.38 to 20 μm spectral region.[16]

Table 6. Major spectra-structure correlations are useful for determining classes of molecules.

Wavenumbers (cm^{-1})	Molecular Structure
4220 - 3680	HF
3700 - 3100	OH, NH, and CH
3100- 3000	Aryl, olefinic, and three membered ring CH
3100 - 2400	Acidic and strongly bonded hydrogens
3000 - 2700	Aliphatic CH
2600 - 2100	SH, BH, PH, and SiH
2300 - 1900	XY and XYZ
2000 - 1700	Aryl and olefinic overtones
1900 - 1550	CO
1700 - 1550	CC and CN
1660 - 1500	NH_2, NH_3^+, and CNH
1660 - 1450	NO
1620 - 1420	Aromatic and heteroaromatic rings
1500 - 1250	CH_3 and CH_2
1470 - 1310	B-O, B-N, NO_3^-, CO_3^{2-}, and NH_4^+
1400 - 1000	SO_2, SO_3^-, SO, and SO_4^-
1350 - 1150	CH_2 and CH wag
1350 - 1120	CF_3 and CF_2
1300 - 1140	P=O
1300 - 1000	C-O
1100 - 830	Si-O and P-O
1000 - 600	Olefinic CH wag
900 - 700	Aromatic CH wag
830 - 500	CCl, CBr, and CI

1.6.2 Source Gas Spectra Measured for this Program

To obtain the spectra of eight gases of interest which are not in the Digitized Reference Library, P. Hanst of Infrared Analysis, Inc., obtained the gases and performed FTIR measurements with 0.5 cm^{-1} resolution at total pressures of one atmosphere. The gas spectra are shown in Figures 13 and 14. His comments on the measurement procedures follow.

Dodecane. The vapor pressure was too low for the standard manometer pressure measurement in a 10 cm cell. Three µl of liquid dodecane was vaporized into a stream of nitrogen flowing into a 144 m long cell, with a 100 l volume, until one atmosphere pressure was obtained.

Nitrogen tetroxide. This dimer only exists in equilibrium with the nitrogen dioxide monomer. The Digitized Reference Library NO_2 spectrum was subtracted from the measured spectrum to obtain the N_2O_4 spectrum.

Sulfur chloride. This compound is hard to handle because it fumes in air to HCl, SO_2, and S. The pure compound was quickly transferred to an evacuatable glass bulb, frozen in liquid nitrogen and the air pumped off. The sample was then warmed and the vapor flowed into a 10 cm cell. HCl and SO_2 vapors were mixed with the sulfur chloride and dimensioned by their distillation concentration. The HCl and SO_2 bands from the Digitized Reference Library were subtracted from the measured spectrum to obtain the S_2Cl_2 spectrum.

Thionyl chloride. This compound also fumed in air and was handled in the same manner as sulfur chloride. After distillation, a clean spectrum was obtained.

Tributyl Phosphate. This compound produced so little vapor that the liquid had to be placed in a glass U-tube closely attached to the 144 m long cell and then, unlike for dodecane, heated while nitrogen was flowing over it and into the cell. The 50 ppm-m value was estimated by comparing the size of the C-H band at 2900 cm^{-1} with the size of the C-H band in the Digitized Reference Library spectrum of n-butanol. It was assumed that the tributyl phosphate with its three butoxy groups should have a C-H band three times as strong as the C-H band in n-butanol.

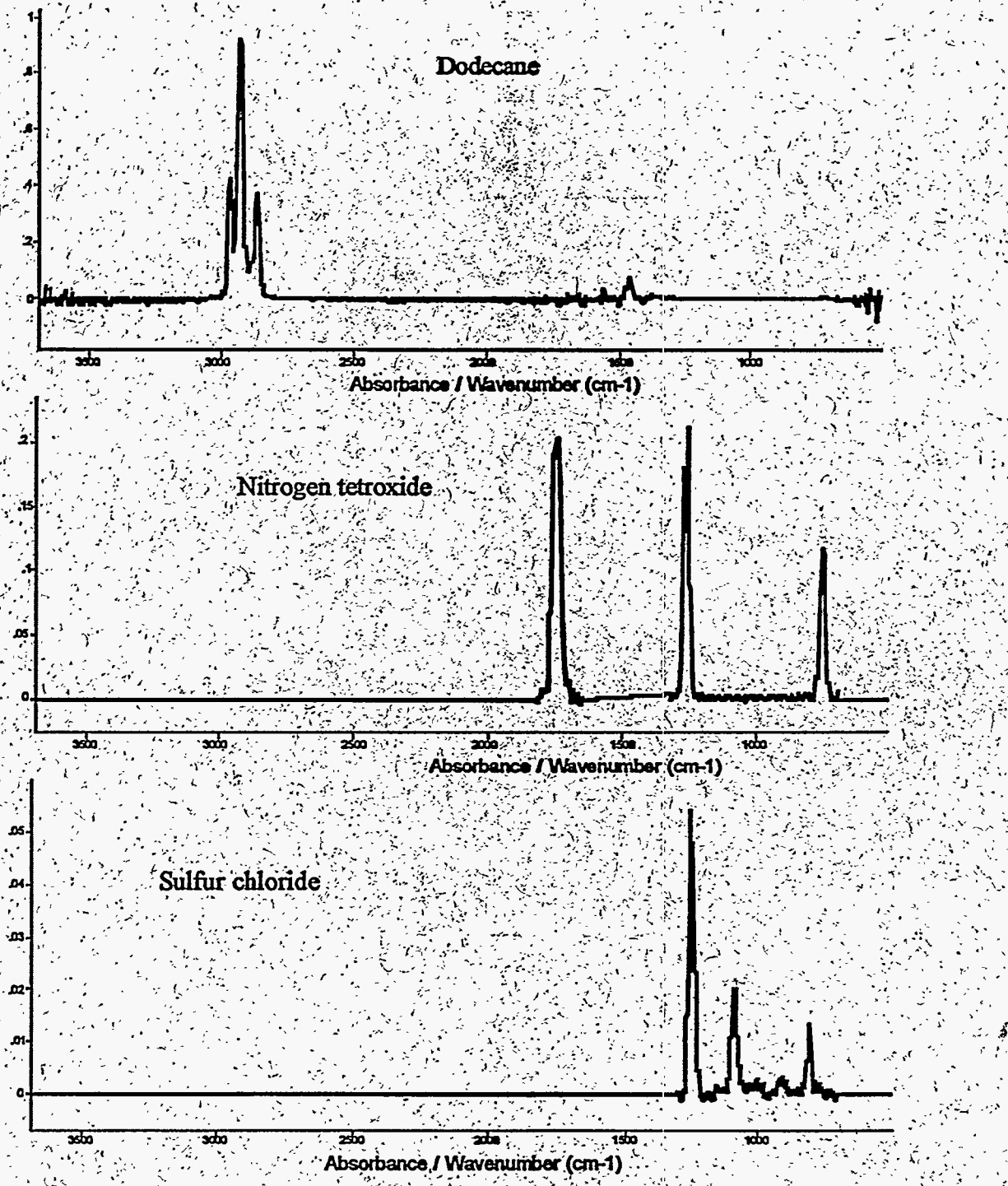

Figure 13 — Measured spectra of Dodecane (310), Nitrogen tetroxide (120), and Sulfur chloride (370).

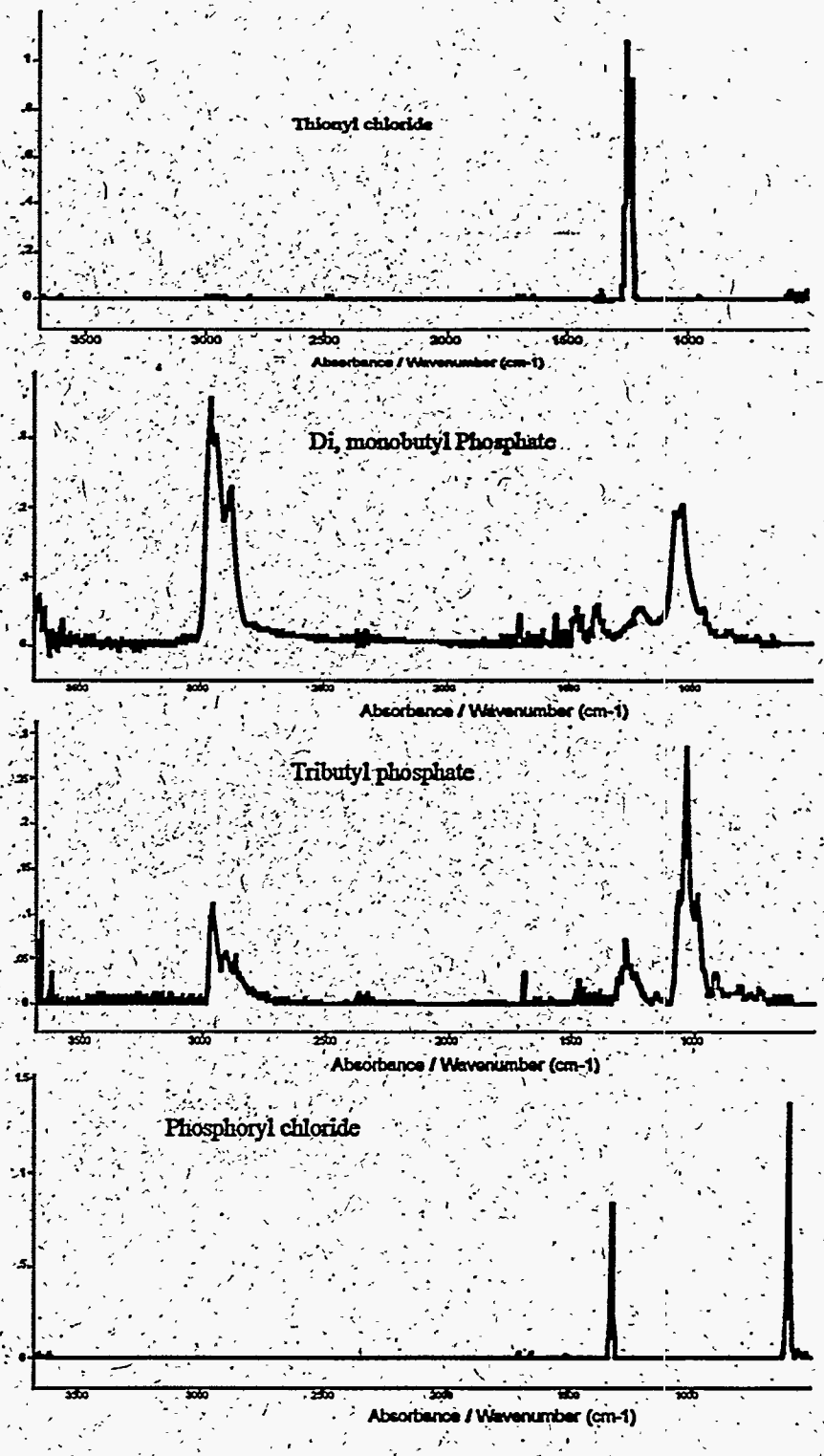

Figure 14 — Measured spectra of Thionyl chloride (770), 55% dibutyl Phosphate + 45% monobutyl Phosphate (500), tributyl Phosphate (50), and Phosphoryl chloride (160).

Dibutyl and monobutyl Phosphates. We were unable to obtain pure samples of these compounds separately but had to use 55% dibutyl phosphate mixed with 45% monobutyl phosphate. The vapor pressure was obtained in the same manner as for tributyl phosphate and the 500 ppm-m value also obtained in the same manner.

Phosphoryl chloride. Fuming in air was a problem but the vapor pressure was high enough for measurements in a 10 cm cell with the subtraction of some impurity bands.

With these measurements of eight source gases and the thirty-one in the Digitized Reference Library plus the atmospheric gas spectra in the same library, forty-two digitized spectra are available for analysis.

1.7 SPECTRAL LINES

In detecting a source gas and measuring its concentration, two general features must be considered: the absorbance of the source gas and the absorbance of normal atmospheric gases at the same wavelength. For the best results, the absorbance of the source gas should be high and the absorbance of the atmospheric gases should be low. To satisfy the former criterion, only spectra peaks of source gases are considered and to satisfy the latter criterion, only spectra peaks of source gases are considered which do not lie within the spectra widths of any atmospheric gas peaks. Source gas peaks which satisfy both criteria are called "tag peaks" or "tag lines" since they have the highest probability for uniquely identifying the source gas under normal atmospheric conditions.

1.7.1 Peak Identification

The **Lab Calc** program automatically identifies peaks in digitized spectra and determines their properties such as peak absorbance, width, and area. Several options in the computational methods and print outs are available. Described here are the options we selected for the spectra analysis.

The "Normal" peak picking method, selected for its high accuracy, identifies peaks by a change in the sign of the second derivative. It rejects all negative peak values and all peaks with slopes less than an operator-specified minimum slope. We set the minimum slope to 0 which minimizes the number of peaks rejected.

Before applying the "Normal" peak picking method, the spectra data is smoothed by averaging every N_a data points into a single value, without modifying the spectrum trace which is nominally composed of 10,000 data points or more. This smoothing eliminates most noise spikes but the N_a value, which must be an odd number, should be low so as not to eliminate real peaks. We smoothed with $N_a = 3$.

The sensitivity rejection parameter sets the noise level for identifying peaks in a trace. A sensitivity level of 5% specifies that 5% of all local maxima in the trace are greater than the noise and

are therefore real peaks. We selected a sensitivity level of 100% which specified that all peaks identified by the "Normal" peak picking method should be considered as real peaks.

The threshold rejection parameter sets the minimum height for peaks to be included in the Peaks Table. We set the absorbance threshold at 0.0001, which is 0.1% of the highest absorbance in the digitized spectra. This parameter eliminates small amplitude noise spikes as well as very weak lines. An example trace showing the peak identifications with a threshold value of 0.1 is shown in Figure 15. In this example, there are only two peaks, Peak 1 and Peak 2, with values above the threshold value.

Peak edges are initially set where the absolute value of the slope on either side of an identified peak is greater or equal to the specified minimum slope. The minimum slope value of 0 we selected maximizes the peak widths. However, "shoulder peaks", peaks that are overlapped on the front or the tail of a larger peak, require special care. In the "Normal" peak picking method, the peak edge locations of shoulder peaks are refined by finding a line that is tangent to the trace on both sides of the identified peak. The peak edges are defined by where the tangent line touches the trace. Figure 15 contains examples of peak edges and base lines drawn for an isolated peak, Peak 1, and for a peak, Peak 2, having a shoulder peak modifying its peak edges.

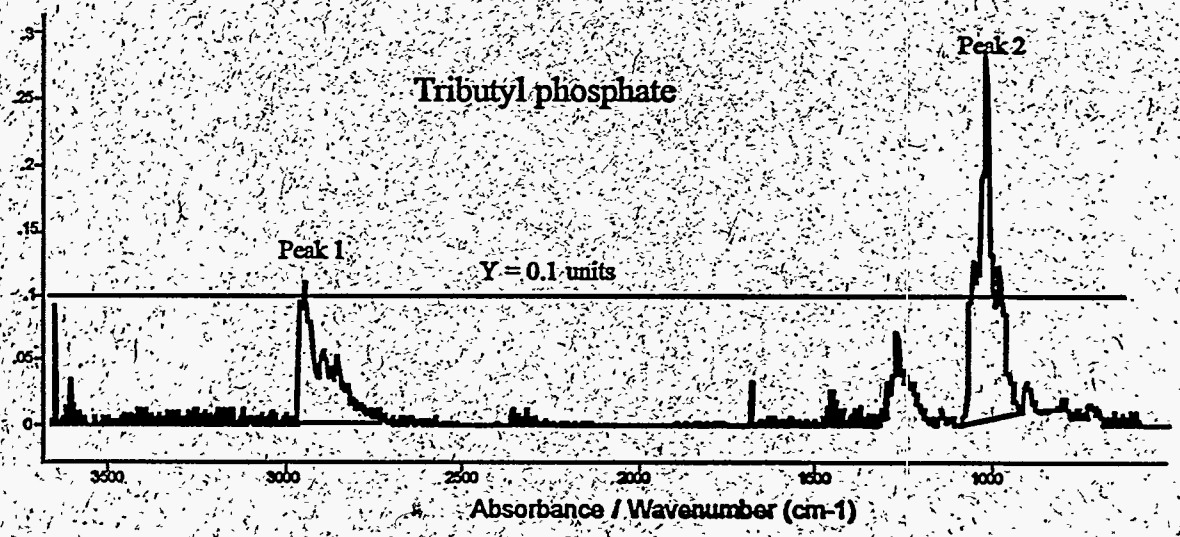

Figure 15 — Only peaks above the threshold value (—) are identified. The vertical tick marks denote the edges of the identified peaks and each solid line connecting the trace between the peak edges is the base-line.

Peak areas are calculated between the peak edges by the trapezoidal rule for integration. An area reject parameter rejects all areas below the operator-specified value. We set the parameter to 0 so as to include all peaks.

Peak areas are normally calculated from the trace height above the base line. However, the valleys between peaks do not always drop back to the original base line. In this case, the calculated area will be in error. To more accurately determine the area, peaks lying close to each other can be grouped together and the base line defined by a common base line that extends from the beginning edge of the first peak to the ending edge of the last peak. The areas of the grouped peaks are calculated by dropping vertical lines from the peak edges down to the group base line. This refinement is illustrated in Figure 16.

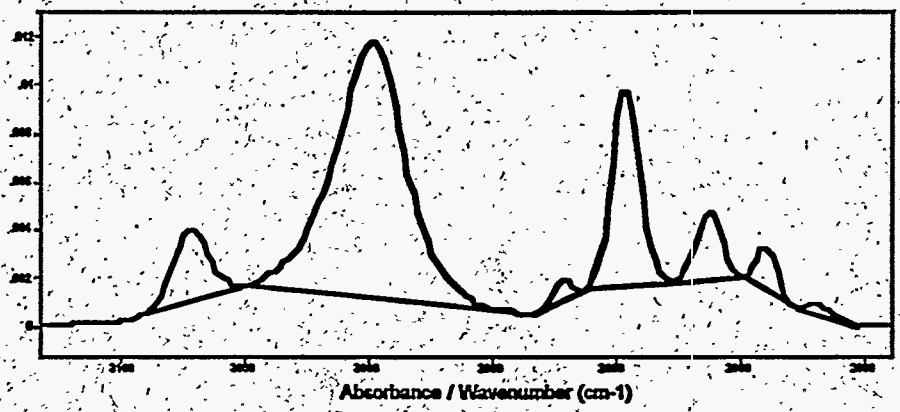

Without Peak Grouping

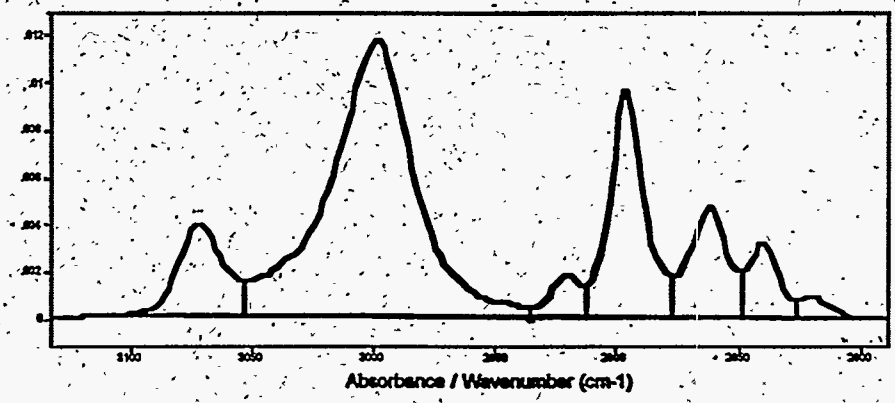

With Peak Grouping

Figure 16 — To determine accurate areas, close-lying peaks must be grouped together and a common base line determined. The areas determined with and without peak grouping are obviously different.

To specify which peaks should be grouped together, a maximum group peak separation parameter is used. Twice the larger half-width[2] of each identified peak is compared to the larger half-width of the adjacent peak. The peak separation parameter specifies a percentage of the smaller of these two values. If the adjacent edges of the two peaks are separated by less than this value, the two constitute a group and are given a common base line. We used 100%. Thus, if two peaks had maximum half-widths of 1 cm^{-1} and 1.5 cm^{-1}, respectively, they would be grouped together if their adjacent edges were closer than 2 cm^{-1}.

The area calculation must also be modified for shoulder peaks. If a large peak has a long tail with a much smaller peak "riding" on top of it, most of the area under the trace belongs to the large peak. Shoulder peaks are identified by three criteria: (1) the shoulder and large peak must be within the same group of peaks, (2) a shoulder peak must have a significantly higher absorbance at one edge than at the other edge, and (3) the height of the shoulder peak above the common valley with the large peak must be much smaller than the height of the large peak above the same valley. In the third criteria, how much smaller is specified by the shoulder ratio setting which we set at 33%. This setting specified that the heights of shoulder peaks must be less than 33% of the peak absorbance of the large peak.

The areas of shoulder peaks are calculated by drawing a skimmed base line from the beginning edge to the ending edge of the shoulder peak. We selected the default exponential base line. The remaining area between the shoulder peak base line and the group base line is considered to be part of the large peak. This base line modification for shoulder peaks is illustrated in Figure 17.

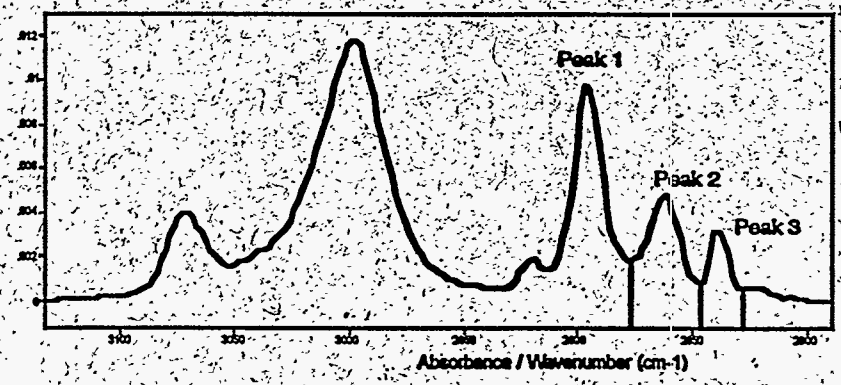

Without Base Line Modification

[2]Lines are often not symmetrical, which means that the two half-widths measured from peak center are not the same.

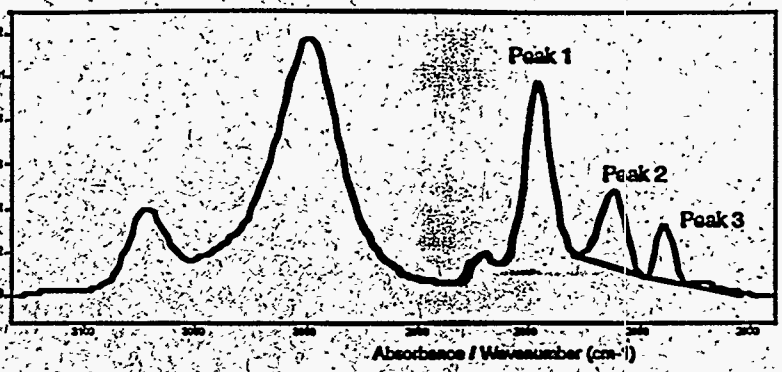

With Base Line Modification

Figure 17 — To determine accurate areas of shoulder peaks, the shoulder peak must have its base line modified as illustrated. The two areas are quite different.

1.7.2 Peak Tables

The peak identification method just described was applied to all 42 spectra in Figures 1 through 14, over their entire spectra range. The Lab Calc-produced Peaks Table for each spectrum was then transformed by the PEAKTB Program into a Modified Peaks Table in which all positive peaks above the threshold level (usually 0.0001) and below the maximum level (usually 1.0) are ordered from the highest to the lowest wavelength.

Carbon tetrachloride is a good gas to illustrate the different Peaks Tables because it has a simple spectrum, shown in Figure 4, with only 15 peaks. Its Modified Peaks Table is shown in Figure 18. The header lines in the table specify the resolution in cm^{-1} and the interval over which the spectrum was measured. The original concentration-path length (cL) value of the measurements is given as well as the operator-specified present value to which the absorbance and area are scaled. The threshold and maximum absorbance values are given in the final header line. For each peak, its number, peak absorbance, and wavelength are given in the first three columns. The next five columns describe the extent of the line: the wave number of (1) the left edge, (2) the peak (called the center), (3) the right edge, and (4) the width of the line. The last column gives the area under the line which is a measure of its strength.

The PEAKTB Program also produces the Sorted Peaks Table in which peaks in the Modified Peaks Table are sorted to list the peaks from the highest to the lowest peak absorbance. The Sorted Peaks Table for carbon tetrachloride is shown in Figure 19. This table is very useful in locating the high absorbance peaks in complicated spectra which have hundreds of peaks. Note that the Peak Number in the Modified and Sorted Peaks Tables is simply a sequence number and not a property of the peak.

CARBON TETRACHLORIDE

Resolution: 2 cm^{-1}. The spectrum interval is 388 to 3700 in wavenumbers. The original cL value is 27.0 ppm-m. The minimum absorbance is 0.0001 and the maximum absorbance is 1.0000.

Peak	Absorb.	Lambda, mm	Line: left	Center	Right	Width	Area
1	0.00471	19.694	509.1	507.8	507.6	1.5	0.00251
2	0.01554	13.073	766.7	764.9	756.7	10.0	0.00904
3	0.01981	13.000	771.1	769.2	730.1	41.0	0.2637
4	0.02392	12.935	774.9	773.1	771.1	3.8	0.0785
5	0.02138	12.831	784.9	779.4	774.9	10.0	0.2005
6	0.1389	12.582	840.3	794.8	784.9	55.4	1.3954
7	0.00012	2.753	3634.0	3632.2	3629.0	5.0	0.0007
8	0.00035	2.748	3642.2	8639.2	3628.9	13.3	0.00162
9	0.00028	2.743	3647.2	8645.6	3642.2	5.0	0.00043
10	0.00047	2.737	3656.0	3653.3	3647.2	8.8	0.00073
11	0.00068	2.732	3663.8	8660.6	3656.1	7.7	0.00182
12	0.00112	2.723	3675.3	3672.6	3668.2	7.1	0.00112
13	0.00224	2.714	3685.1	3684.4	3683.1	2.0	0.00022
14	0.00377	2.710	3690.8	3690.2	3688.8	2.0	0.00022
15	0.0104	2.705	3696.2	3696.2	3694.3	1.9	0.00002

Figure 18 — Modified Peaks Tables give key line information in which the peaks are ordered from the highest to lowest wavelength.

CARBON TETRACHLORIDE

Resolution: 2 cm^{-1}. The spectrum interval is 388 to 3700 in wavenumbers. The original cL value is 27.0 ppm-m. The minimum absorbance is 0.0001 and the maximum absorbance is 1.0000.

Peak	Absorb.	Lambda, mm	Line: left	Center	Right	Width	Area
1	0.1389	12.582	840.3	794.8	784.9	55.4	1.3954
2	0.02392	12.935	774.9	773.1	771.1	3.8	0.0785
3	0.02138	12.831	784.9	779.4	774.9	10.0	0.2005
4	0.01981	13.000	771.1	769.2	730.1	41.0	0.2637
5	0.01554	13.073	766.7	764.9	756.7	10.0	0.00904
6	0.0104	2.705	3696.2	3696.2	3694.3	1.9	0.00002
7	0.00471	19.694	509.1	507.8	507.6	1.5	0.00251
8	0.00377	2.710	3690.8	3690.2	3688.8	2.0	0.00022
9	0.00224	2.714	3685.1	3684.4	3683.1	2.0	0.00022
10	0.00112	2.723	3675.3	3672.6	3668.2	7.1	0.00112
11	0.00068	2.732	3663.8	8660.6	3656.1	7.7	0.00182
12	0.00047	2.737	3656.0	3653.3	3647.2	8.8	0.00073
13	0.00035	2.748	3642.2	8639.2	3628.9	13.3	0.00162
14	0.00028	2.743	3647.2	8645.6	3642.2	5.0	0.00043
15	0.00012	2.753	3634.0	3632.2	3629.0	5.0	0.0007

Figure 19 — Sorted Peaks Tables give key line information in which the peaks are ordered from the highest to lowest absorbance.

1.7.3 Highest Non-Interfered Peaks

From the Sorted Peaks Tables, the highest absorbance peaks are always Peak No. 1. By linearly scaling these highest absorbance peaks to the same concentration, say 1000 ppm-m, the relative detection potentials of the gases are obtained. Table 7 lists these peaks for the gases of interest as well as for the atmospheric gases. The absorbance and wavelength at the peak center is given for each gas, as is the total number of peaks, or lines, detected from the digitized spectra for peak absorbances above 0.0001[3] (0.1% of the highest peak absorbance which is usually between 0.1 and 0.3). The number of peaks in a spectrum is a rough measure of the spectrum complexity -- the 41 spectra produced 7,904 peaks. This table is important because it indicates the relative detection probabilities and gives the best wavelengths for accurate measurements of gas concentrations when the atmosphere is not important, i.e., when the monitor is close to the plume.

When the plume is at a distance, atmospheric absorption must be considered. This effect is negated for each gas of interest by comparing its Sorted Peaks Table to the Modified Peaks Table for each atmospheric gas listed in Table 3, i.e., H_2O, CO_2, CH_4, N_2O, and CO. For each gas, the highest absorbance line which does not overlap an atmospheric line is taken as the "tag" peak, i.e., the line which is "uniquely" identifies the gas. To be a tag line, we specified that the line could not lie anywhere within the width of any peak in the atmospheric gas spectra. This stringent requirement does not guarantee the selection of a high absorbance tag line, but it has a high probability of eliminating atmospheric interferences, leaving only the less troublesome continuum absorption.

The tag lines are listed in Table 8 in order of absorbance values. Tag lines which would be detected with a far-infrared focal plane array are listed in Table 8 in the normal font and tag lines which would be detected with a mid-infrared focal plane array are listed in italics. The majority of gases would be identified with the far-infrared array, e.g., HgCdTe, and a few would be identified with the mid-infrared array, e.g., InSb.

[3] To eliminate noise spikes, this threshold was slightly higher for most of the gases measured on this program.

Table 7. Number of peaks and the maximum absorbance line at 1000 ppm-m for each gas surveyed, assuming no atmospheric effects.

Chemical Name	Absorbance	, μm	No. Lines
Phosphoryl chloride	8.542	16.711	65
Tributyl phosphate	5.684	9.680	356
Carbon tetrachloride	5.144	12.582	15
Nitrous acid	4.585	7.913	31
Benzene	3.881	14.846	21
Dodecane	2.965	3.411	145
Hydrogen cyanide	2.513	14.033	135
Carbon dioxide	2.078	14.974	85
Nitrogen tetroxide	1.753	7.931	323
Nitrogen dioxide	1.455	6.142	505
Thionyl chloride	1.414	7.969	119
o-Xylene	1.366	13.496	131
Nitrous oxide	1.309	4.473	22
n-Pentane	1.130	3.372	99
Hydrogen fluoride	1.029	2.476	181
Ammonia	1.004	10.345	448
Hexane	1.000	3.373	47
Nitric acid	0.949	5.843	102
Trichloroethylene	0.902	11.772	217
Dichlorodifluoromethane	0.882	13.340	64
Sulfur dioxide	0.870	7.350	80
Kerosene	0.850	3.370	84
Butane	0.842	3.372	125
Toluene	0.826	13.723	75
4-methyl 2-Pentanone	0.798	5.771	80
Methane	0.738	3.314	422
Methanol	0.721	9.678	193
Dibutyl + Monobutyl phosphate	0.707	3.370	392
2-Butanone	0.678	5.731	488
m-Xylene	0.525	13.020	270
Butanol	0.444	3.370	507
p-Xylene	0.351	12.575	172
Phosphorous trichloride	0.325	19.713	12
Hydrogen peroxide	0.272	7.747	25
Hydrazine	0.212	10.442	399
Hydrogen chloride	0.174	3.396	408
Carbon monoxide	0.149	4.603	53
Sulfur chloride	0.147	7.969	265
Water	0.139	6.050	341
Nitrogen oxide	0.077	5.254	68
Hydrogen sulfide	0.003	2.636	334

Table 8. Tag line and absorbance properties at 1000 ppm-m of each gas for which there are no interfering atmospheric lines.

Chemical Name	Absorbance μm		Width	Line cm^{-1}
No.				
Tributyl phosphate	9.680	5.684	43.6	1
Carbon tetrachloride	12.582	5.144	55.4	1
Nitrous acid	11.731	2.829	7.4	2
Trichloroethylene	11.772	0.902	33.9	1
Ammonia	10.741	0.841	22.9	2
Dichlorodifluoromethane	13.092	0.764	30.9	2
Hydrogen fluoride	2.499	0.741	5.9	4
Methane	3.314	0.738	25.8	1
Methanol	9.678	0.721	9.7	1
m-Xylene	13.020	0.525	30.3	1
Nitric acid	11.382	0.467	4.0	12
Di + Monobutyl phosphate	9.608	0.409	2.1	23
p-Xylene	12.575	0.351	48.7	1
2-Butanone	8.552	0.298	2.8	5
Hydrogen cyanide	2.999	0.232	2.8	2
Butanol	9.349	0.206	83.0	8
Hydrazine	10.631	0.196	10.3	2
o-Xylene	3.361	0.182	16.1	7
Dodecane	3.514	0.135	4.5	17
Nitrogen tetroxide	12.940	0.083	2.0	41
4-methyl 2-Pentanone	8.877	0.072	14.6	18
Sulfur dioxide	8.597	0.069	3.2	13
Benzene	9.639	0.066	46.7	17
Sulfur chloride	9.144	0.055	26.0	4
Toluene	9.692	0.046	5.3	27
Nitrogen dioxide	13.187	0.034	15.4	34
n-Pentane	10.928	0.021	25.1	23
Butane	10.455	0.017	20.8	21
Thionyl chloride	4.015	0.016	21.6	35
Hexane	8.722	0.011	63.6	18
Kerosene	9.166	0.010	37.8	38
Nitrous oxide	3.922	0.008	43.2	15
Hydrogen chloride	3.771	0.005	12.6	63
Nitrogen oxide	5.131	0.003	2.2	49
Hydrogen sulfide	2.599	0.002	2.9	11

The line number in Table 8 indicates the amount of atmospheric interference to that gas. For example, the trichloroethylene tag line is line #1 from the Sorted Peaks Table, i.e., there are no atmospheric interferences for trichloroethylene. On the other hand, the toluene tag line is line #27 from the Sorted Peaks Table, i.e., atmospheric gases interfere with the 26 lines with higher absorbances. The line widths give an indication of how large the tag line is.

As seen in Table 8, seven of the gases had no atmospheric interference. Not surprisingly, methane was the main atmospheric interferent due to its very large number of lines from its C-H stretch vibrations in the 2.7 to 3.8 μm region and other lines in the 5.0 to 8.6 μm region. The second most prevalent interferent was water with its many vibrational lines in the 2.5 to 3.3 μm region, in the 4.8 to 7.9 μm region, and in the 15.7 to 19.6 μm region. Carbon dioxide was the third most prevalent interferent, obstructing emissions in the 4.2 to 4.4 μm region and in the 13.9 to 19.9 μm region. In particular, methane interfered with 27 gases of interest, water with 23 gases of interest, and carbon dioxide with 16 gases of interest. Nitrous oxide only interfered with 2 gases and carbon monoxide with one.

Three gases have emission lines which are always overlapped with atmospheric emission lines:

- Phosphoryl chloride
- Hydrogen peroxide
- Phosphorous trichloride

Their concentrations cannot therefore be unambiguously measured without first removing atmospheric emission lines by carefully and accurately determining their concentrations – a time-consuming task – and even then the interferences place a lower bound on the measurable concentrations.

1.8 RELATIVE DETECTION PROBABILITY

Identification of the tag line for each source gas locates the wavelength which maximizes the probability of detecting low concentrations of that gas in the open atmosphere. The next step is to identify those gases which have the highest probability of detection relative to the other source gases, thereby providing a rank ordering of the gases according to their probability of detection. Such rank ordering is advantageous for AOTF-based spectrometers which measure spectra sequentially because it allows fast searching of an area for tell-tale gases by concentrating on the gases with the highest probabilities of detection. There are two cases of interest: thick plumes and thin plumes, where thick and thin are defined by their optical thickness, i.e., optical absorption.

1.8.1 Thick Plume Detection

The exact probability of detection for a source gas depends on several factors, such as the gas's absorbance, temperature, and wavelength, as well as on the receiver's collector area and optical transmission. Some factors depend only on the optical design and will not change appreciably for the different gases. These factors can therefore be represented by a constant K_1 and the power density on the receiver's detector from gaseous emissions can be written as:

$$P_r = K_1 P \tag{6}$$

$$P = W \tag{7}$$

where is the emissivity at the wavelength , W is the spectral blackbody emittance in W/cm^2 µm, and is the AOTF passband in µm.

The Planck radiation law provides the W functionality as:[1]

$$W = c_1 / ^5 [\exp(c_2/T) - 1] \tag{8}$$

in W/µm cm^2 where T is the blackbody temperature of the gas and

$$c_1 = 3.7415 \times 10^4 \quad \text{W µm}^4 / \text{cm}^2 \tag{9}$$

$$c_2 = 1.4388 \times 10^4 \quad \text{µm deg} \tag{10}$$

The passband of an AOTF is constant in wavenumbers, not in wavelengths. The relationship between them is given by

$$= 10^{-4} {}^2 \Delta\nu \tag{11}$$

where is the AOTF passband in cm^{-1}. For an optically thick plume,

$$= 1.0 \quad \text{nality as:}^1 \tag{12}$$

which reduces Eq. 6 to

$$P = 3.7415 / ^3 [\exp(c_2/T) - 1] \tag{13}$$

for the normalized power density incident on the detector from that fraction of the blackbody radiation from the source gas passed through by the AOTF.

Values of this normalized power density for a 25 C plume are given in Table 9 for the source gases of interest at their tag line wavelengths. The values are relatively large for the long wavelengths but decrease rapidly for wavelengths below 8 μm and almost vanish below 3 μm, due primarily to the large falloff of the blackbody radiation curve at the short wavelengths but aided by the lower fractional passband of the AOTF at the shorter wavelengths. It follows from Eq. 9 that the wavelength at which the normalized power density is peaked is given by

$$\text{peak} = 4796 / T \quad T < 4796 \tag{14}$$

The peak wavelength for a 25C plume is 16.09 μm. For the peak wavelength to be even as low as 12 μm the plume temperature would have to be 126C! Plume radiance clearly favors far-infrared wavelengths, discriminating strongly against the mid-infrared and near-infrared wavelengths.

Although a high power density from the plume is needed at the detector, it is not sufficient. The detector noise must also be low to provide a high signal-to-noise ratio. The noise power at the detector is given by

$$P_n = [A_d f]^{1/2} / D^* \tag{15}$$

$$= K_2 / D^* \tag{16}$$

where A_d is the area of the detector and f is the electrical noise bandwidth in Hz, collected together in the design constant K_2. The detector detectivity is a function of wavelength and detector material. For the far-infrared the most common material is HgCdTe and for the mid-infrared the most common material for sensitive detection is InSb. Nominal D* values for these detector materials are:

$$D^* = (2 \times 10^{10})\, \lambda / 14 \quad \text{HgCdTe} \tag{17}$$

$$D^* = (1 \times 10^{11})\, \lambda / 5 \quad \text{InSb} \tag{18}$$

where the HgCdTe detector would be used for wavelengths from 5 to 14 μm and the InSb detector for wavelengths from 2 to 5 μm. These values are also given in Table 9. The higher sensitivity of the InSb favors the mid-infrared wavelengths.

A relative merit factor is obtained by eliminating the system design details which have little, if any, dependence on the wavelength and including those remaining parameters which determine the signal-to-noise ratio, i.e.,

$$MF_1 = 10^5\, P\, D^* \tag{19}$$

where the 10^5 factor scales the merit factor to values near unity. Values of this merit factor for the source gases of interest are given in Table 9. This merit factor indicates that it would be 10^6 times more difficult to detect a thick plume of dodecane than a thick plume of carbon tetrachloride or p-xylene, etc. It is readily apparent that the higher sensitivity of InSb detectors does not compensate adequately for the rapid decrease of the blackbody radiance at the short wavelengths. Thus, the far-infrared wavelengths are very useful for the detection of source gases in thick plumes whereas the mid-infrared wavelengths are not.

Table 9. Detectivity merit factor for an optically thick gas plume at 25 C.

Chemical Name	P	10^{-11} D*	MF1
	μm	$\mu W/cm^2$	$cm/Hz^{1/2}$ W
Nitrogen dioxide	13.187	43.1	.188	8.12
m-Xylene	13.020	42.7	.186	7.94
Nitrogen tetroxide	12.940	42.5	.185	7.85
Carbon tetrachloride	12.582	41.5	.180	7.45
p-Xylene	12.575	41.4	.180	7.44
Trichloroethylene	11.772	38.7	.168	6.50
Nitrous acid	11.731	38.5	.168	6.46
Nitric acid	11.382	37.1	.163	6.03
n-Pentane	10.928	35.1	.156	5.47
Ammonia	10.741	34.2	.153	5.24
Hydrazine	10.631	33.6	.152	5.11
Butane	10.455	32.7	.149	4.89
Toluene	9.692	28.5	.138	3.94
Tributyl phosphate	9.680	28.4	.138	3.93
Methanol	9.678	28.4	.138	3.92
Benzene	9.639	28.2	.138	3.88
Dibutyl phosphate	9.608	28.0	.137	3.84
Monobutyl phosphate	9.608	28.0	.137	3.84
Butanol	9.349	26.4	.134	3.52
Kerosene	9.166	25.2	.131	3.31
Sulfur chloride	9.144	25.1	.131	3.28
4-methyl 2-Pentanone	8.877	23.4	.127	2.97
Hexane	8.722	22.4	.125	2.79
Sulfur dioxide	8.597	21.6	.123	2.65
2-Butanone	8.552	21.3	.122	2.60
Dichlorodifluoromethane	13.094	2.9	.187	2.45
Thionyl chloride	4.015	0.348	.803	0.28
Nitrous oxide	3.922	0.281	.784	0.22
Nitrogen oxide	5.131	0.228	.073	0.17
Hydrogen chloride	3.771	0.193	.754	0.15
Dodecane	3.514	0.094	.703	0.07
o-Xylene	3.361	0.057	.672	0.04
Methane	3.314	0.049	.663	0.03
Hydrogen cyanide	2.999	0.014	.600	0.01
Hydrogen sulfide	2.599	0.002	.520	0.00
Hydrogen fluoride	2.499	0.001	.500	0.00

1.8.2 Thin Plume Detection

For an optically thin plume, the emissivity is not unity but has a value which depends on the molecular concentration, optical absorptivity, and plume thickness. From Kirchhoff's law emissivity is equal to absorption. For a gas this law is expressed mathematically as:

$$= 1 - \exp(-kL) \qquad (20)$$

where L is the path length through the plume and k is the absorption coefficient of the gas. It can be shown from the definition of absorbance (the logarithm of the input intensity relative to the output intensity) and the ideal gas law that

$$k = 22.8\, a_1\, P_V \qquad (21)$$

where a_1 is the source gas absorbance at 1000 ppm-m and P_V is its vapor pressure in atmospheres.

The plume length is arbitrary. We select a value of 0.1 cm to make relative comparisons among the numerous source gases because the emissivities then vary considerably among the gases and because the concentration-path length product is conveniently given by

$$NL = P_V \qquad 1000 \text{ ppm-m} \qquad (22)$$

Thus, the emissivity of ammonia, with a vapor pressure of 9.9 atmospheres, is evaluated at 9,900 ppm-m whereas the emissivity of dodecane, with a vapor pressure of 0.00016 atmospheres, is evaluated at 0.16 ppm-m.

The Clausius-Clapeyron equation relating vapor pressure and temperature can be integrated to relate the vapor pressures at two different temperatures through the heat of vaporization, ΔH_V, to give

$$\log (P_2 / P_1) = H_V (T_2 - T_1) / 4.576\, T_2\, T_1 \qquad (23)$$

At the boiling point, T_{bp}, the vapor pressure is exactly one atmosphere and this equation reduces to

$$\log P_V = H_V (T - T_{bp}) / 4.576\, T\, T_{bp} \qquad (24)$$

Thus, the vapor pressure of an ideal gas can be estimated from its boiling point and heat of vaporization. The known boiling points for the source gases are given in Table 10.[4] Most of the gases

[4]The value for kerosene is an average value and the value for nitrous acid is assumed to be the same as nitrogen dioxide.

also have measured heats of vaporization. Those which do not have measured values could have their heat of vaporization estimated from the empirical relationship:

$$H_V / T_{bp} = 21 \text{ cal / deg mole} \qquad (25)$$

To be slightly more accurate, this ratio was averaged from all measured values in Table 10 with the result that

$$H_V / T_{bp} = 22.1 \qquad (26)$$

which was used in Table 10 when the heat of vaporization was not known.

The calculated vapor pressures at 25C are given in Table 10, as well as measured values when known. Agreement between the calculated and measured values is quite good. The high vapor pressures do not mean that those pressures would actually exist in a vapor plume, but rather that those pressures would cause the plume to rapidly expand into the surrounding atmosphere. The net affect on the NL value would be, to first order, the same as if the high pressure did exist only in the 0.1 cm diameter plume. Thus, the vapor pressures as given are valid for making relative comparisons of vapor pressures from different gases. Thus, volatile gases such as methane and ammonia are thousands of times more likely to exist in high concentrations than is dodecane or the phosphate gases.

The only difference between a thin plume and a thick plume is the emissivity. Thus, the thin plume detectivity merit factor is given by

$$FM_2 = FM_1 \qquad (27)$$

The emissivity for each gas is determined from Eq. 16, using the absorbance value in Table 8 and the vapor pressure in Table 10. The results are given in Table 11 for a 0.1 cm diameter plume.

Table 10. Calculated and measured vapor pressures of each gas at 25C.

Chemical Name	Tbp	$\Delta H_v/Tbp$	Pressure in Torr	
		Kcal/deg mole	Cal.	Meas.
Nitrogen oxide	121.4	27.2	2560000.	———
Methane	111.7	17.5	188000.	———
Nitrous oxide	184.7	21.4	45700.	39800.
Hydrogen chloride	188.2	20.5	34200.	35400.
Hydrogen sulfide	213.6	20.9	15000.	15600.
Ammonia	239.8	23.2	7500.	7520.
Dichlorodifluoromethane	243.3	22.1	5860.	4880.
Sulfur dioxide	263.1	22.7	2900.	3010.
Butane	272.6	19.7	1770.	1810.
Nitrogen tetroxide	294.3	31.0	929.	—
Nitrogen dioxide	294.3	22.1	877.	—
Nitrous acid	294.3	22.1	866.	—
Hydrogen fluoride	292.6	6.2	805.	923.
Hydrogen cyanide	299.2	22.1	731	265.
n-Pentane	309.2	19.9	524.	512.
Hexane	341.9	20.2	171.	152.
Methanol	337.7	24.9	144.	127.
Carbon tetrachloride	349.9	20.4	128.	114.
Benzene	353.2	20.8	110.	95.2
2-Butanone	352.7	21.2	108.	94.5
Thionyl chloride	352.0	22.1	102.	—
Nitric acid	356.2	22.1	87.6	—
Trichloroethylene	360.4	20.8	85.3	74.3
Toluene	383.8	20.7	38.4	28.4
4-methyl 2-Pentanone	389.6	21.2	29.0	19.8
Hydrazine	386.7	25.8	16.0	14.4
p-Xylene	411.5	20.7	14.4	8.89
m-Xylene	412.3	20.7	14.1	8.51
Sulfur chloride	408.8	22.1	12.4	-
Butanol	390.9	26.5	12.1	6.46
o-Xylene	417.6	20.7	11.6	6.61
Dodecane	489.5	22.1	0.616	0.12
Kerosene	523.	22.1	0.175	-
Tributyl phosphate	562.2	22.1	0.041	-
Dibutyl phosphate	613.2	22.1	0.006	-
Monobutyl phosphate	664.2	22.1	0.001	-

Table 11. Detectivity merit factor for a thin gas plume at 25C.

Chemical Name	Emissivity	MF_2
Nitrous acid	0.999	6.451
Carbon tetrachloride	0.828	6.168
Ammonia	1.000	5.242
Dichlorodifluoromethane	1.000	2.449
Nitrogen tetroxide	0.207	1.626
Sulfur dioxide	0.465	1.232
Trichloroethylene	0.182	1.186
Methanol	0.240	0.942
Nitric acid	0.116	0.697
Nitrogen dioxide	0.085	0.690
Butane	0.089	0.434
2-Butanone	0.081	0.210
n-Pentane	0.032	0.172
Nitrogen oxide	1.000	0.167
Hydrogen chloride	1.000	0.146
Nitrous oxide	0.624	0.138
m-Xylene	0.013	0.106
Benzene	0.019	0.073
p-Xylene	0.009	0.069
Hydrazine	0.008	0.043
Methane	1.000	0.032
Toluene	0.004	0.015
Hexane	0.005	0.015
Butanol	0.004	0.014
4-methyl 2-Pentanone	0.004	0.013
Sulfur chloride	0.002	0.007
Tributyl phosphate	0.001	0.003
Thionyl chloride	0.005	0.001
Hydrogen cyanide	0.169	0.001
Dibutyl phosphate	0.000	0.000
Monobutyl phosphate	0.000	0.000
Kerosene	0.000	0.000
Dodecane	0.000	0.000
o-Xylene	0.004	0.000
Hydrogen sulfide	0.068	0.000
Hydrogen fluoride	0.871	0.000

The FM_2 figure of merit is the best one for a relative ranking of the source gases. Thus, under these conditions, ammonia is four orders of magnitude more likely to be detected than hydrogen fluoride and 72 times more likely to be detected than benzene. In fact all gases emitting in the mid-infrared are considerably less likely to be detected than gases emitting in the far-infrared.

1.9 CONCLUSIONS

There are several conclusions which can be drawn from this analysis. The most important ones are:

- Relative detection probabilities for thin plumes at 25C vary from 6.45 for nitrous acid to 0.0004 for hydrogen fluoride with most tag line wavelengths below 8 μm having low probabilities of detection.
- The top ten gases which have the highest probability of detection are:

  nitrous acid
  carbon tetrachloride
  ammonia
  dichlorodifluoromethane
  nitrogen tetroxide
  sulfur dioxide
  trichloroethylene
  methanol
  nitric acid
  nitrogen dioxide

- Spectroradiometer resolutions larger than 0.2 cm^{-1} decrease the measured absorbance of narrower spectral lines but have little effect on broad lines or on closely spaced narrow lines.
- Without atmospheric absorption, source gas absorbances at 1000 ppm-m vary from 8.842 for phosphoryl chloride to 0.003 for hydrogen sulfide.
- Tag line absorbances at 1000 ppm-m vary from 5.684 for tributyl phosphate to 0.002 for hydrogen sulfide.
- Equilibrium vapor pressures vary from 336 atmospheres for nitrogen oxide to 1 x 10-6 atmospheres for monobutyl phosphate.
- Relative detection probabilities for thick plumes at 25C vary from 8.12 for nitrogen dioxide to 0.0005 for hydrogen fluoride with all tag line wavelengths below 8 μm having dramatically lower probabilities of detection.

2. SYSTEM DESIGN AND ANALYSIS

2.1 AOTF PERFORMANCE ANALYSIS

The major risk element in the system is the AOTF, and in general the resolution and efficiency are degraded due to crystal quality limitations. At low resolution, the crystal quality limitations are less restrictive, and the AOTF can approach theoretically limited performance. This is illustrated by the measured response of a noncollinear TAS AOTF to a 10.6 μm laser beam, as shown in Figure 20. This AOTF has an interaction length of 1.5 cm, and a calculated resolution of 7.5 cm^{-1}. The resolution was measured by sweeping the AOTF response over the laser line, and the measured resolution was 7.9 cm^{-1}, and the response curve very nearly matches the theoretical $sinc^2$ response function. The efficiency was measured as 2% with 0.2 W/cm^2 of applied acoustic intensity, which closely matches the predicted value of 0.224 W/cm^2 at this efficiency. Therefore at low resolution, the AOTF has nearly theoretically limited performance.

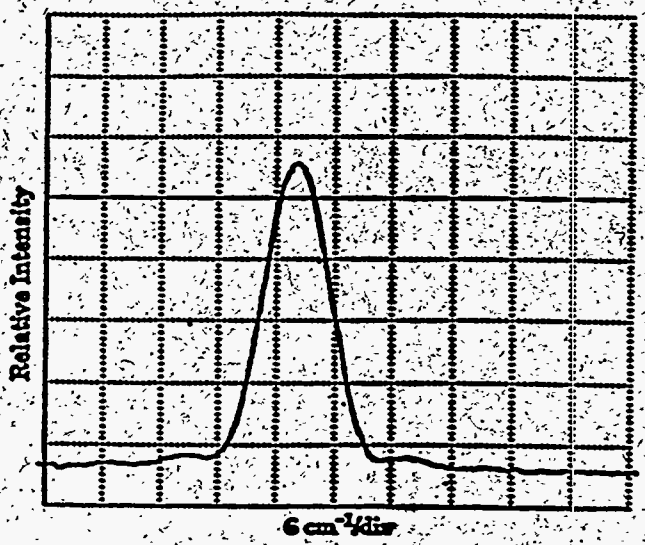

Figure 20 — Response of low resolution AOTF showing nearly theoretically limited performance.

At higher resolution, the TAS crystal quality limitations become more severe. This can be seen from the collinear AOTF response to the 10.6 μm laser beam, as shown in Figure 21. This AOTF has an interaction length of 5 cm, and was operated in a double pass configuration, and the input and output beams were separated using birefringent reflection from an internal wedge angle in the AOTF. The

calculated resolution for this AOTF is 1 cm^{-1}, and the efficiency should be 50% at 0.5 W/cm^2. The measured resolution was 2cm^{-1} at an efficiency of 10% at 0.5 W/cm^2. The resolution was therefore half the predicted, and the efficiency was less than a quarter. These results are consistent with having an interaction length that is half the actual length, which probably indicates that crystal quality limitations are reducing the effective length by 50%.

The design was based upon these measured values, which were sufficient to produce excellent sensitivities for gas detection. Should a better quality AOTF be produced, the sensitivities will improve over the calculated design values, and it is possible that the sensitivities could improve as much as a factor of five for a theoretically limited AOTF.

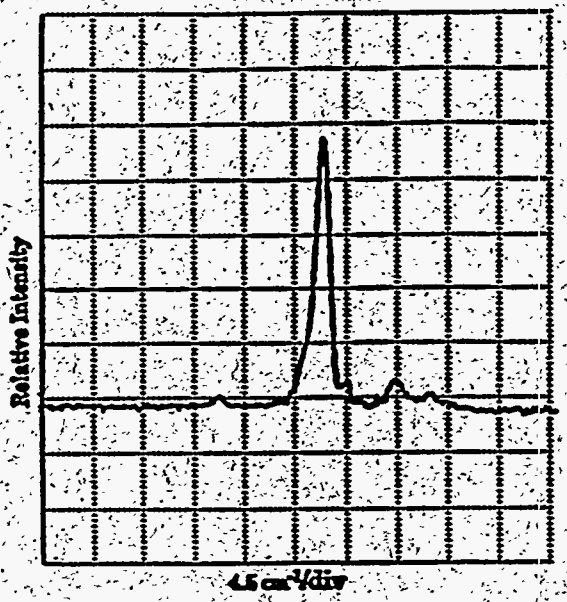

Figure 21 —Response of high resolution TAS AOTF with acceptable, although not theoretically limited performance.

2.2 SYSTEM LAYOUT AND COMPONENT SELECTION

The system design objective was to operate on both the 2-5 μm and 8-12 μm bands, and several design concepts were examined. Design tradeoffs for the AOTF filter were conducted, in which either separate AOTFs could be used for the two bands, or a single AOTF with special beam splitters to direct the output to the detector arrays would be designed. Both concepts were feasible, although the single AOTF system involved considerably more risk. Not only were the chromatic beam splitters lossy, but the transducer for the AOTF would have to cover two separate frequency ranges.

The AOTF must have a resolution of 2 cm^{-1} to adequately resolve the spectra, which requires the use of a collinear AOTF. For a collinear TAS AOTF, the frequency range for the 8-12 μm band is 15 to

24 MHz, which is a bandwidth covering 46% of the center frequency, and is easily achievable. For the 2-5 μm band, the frequency range is 38 to 95 MHz, which covers 86% of the center frequency, and although more difficult than the long wave band, is still feasible. In order to cover both bands with one transducer, the transducer thickness could be adjusted to produce the primary resonance for the 8-12 μm band, and the third order resonance could be used for the 2-5 μm band. Another possibility is to apply two separate transducers in a sandwich stack to the AOTF, each of which would be resonant separately over the two bands. Both of these approaches are risky, and would require some development. In conjunction with the added losses of the special beam splitters, it was decided that two AOTFs would be the least risky approach, and the design proceeded along having essentially two separate AOTF and imaging systems.

A layout drawing of the spectrometer system design is shown in Figure 22, and it consists of separate AOTFs for the 2-5 and 8-12 μm systems, both of which have a resolution of 2 cm^{-1}. The systems are linked with a common optical input axis, and the two polarization states of the input beam are separated and directed into the individual systems. Although separate parallel apertures could have been used for the two bands, it was decided to have a common boresighted input axis. This allows for the use of a single telescope to change the field of view simultaneously for both systems.

The AOTF interacts with the input beam, and the polarization of the selected passband is rotated 90 by the AOTF. The signals are then reflected off the beam splitters and into the IR cameras. A wide range of camera systems were examined, including staring and scanned arrays, cooled and room temperature detectors, and commercial and fabricated systems. The criteria used in evaluating the cameras were (1) having an optical throughput that could be matched directly to that of the AOTF, (2) having the best sensitivity and spectral range, and (3) being affordable. Under these conditions, the optimum choices were the Cincinnati Electronics IRC-160 InSb camera for the 2-5 μm band, and the Inframetrics 760 system for the 8-12 μm region.

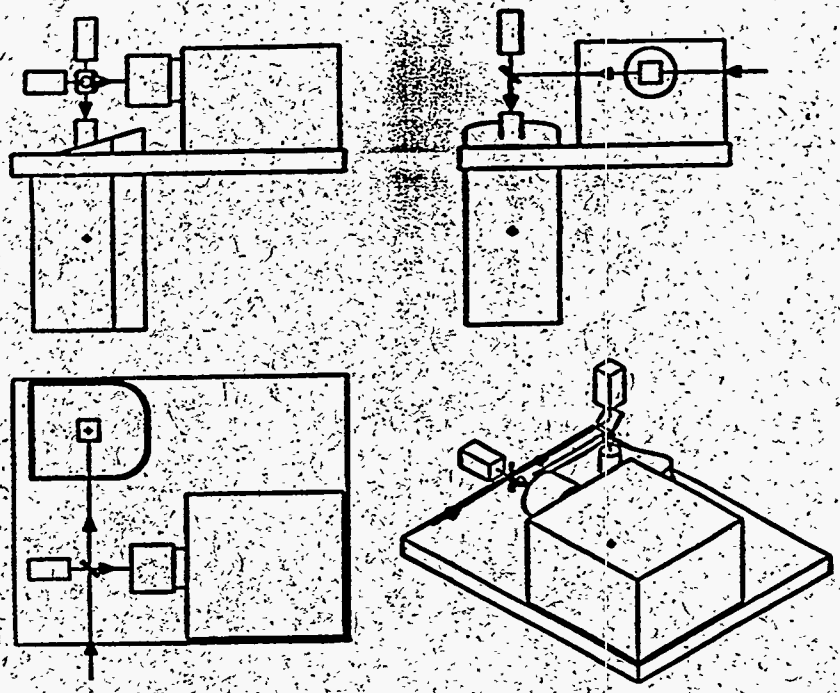

Figure 22 Layout design of dual band AOTF imaging spectroradiometer.

The Cincinnati Electronics IRC-160 is a 120 x 160 staring InSb array with an NET of 0.025K, a spectral range of 2.2 - 4.6 μm, a 12-bit digital output, and a 60 Hz framing rate. The 18.2 x 13.7 field of view with a 25 mm input lens also matches very well to the throughput of the AOTF, which is 17 with a 1-inch aperture.

The Inframetrics 760 camera for the 8-12 μm band is a scanned Hg_1CdTe system with a NET of < 0.2K, a 20 x 15 field of view with 1 inch optics, and a 60 Hz framing rate over an equivalent field of 194 x 200 pixels. The scanning is done with a pair of galvometric mirrors, which are rugged and reported to have a lifetime of several years of continuous operation. The output is available in digital form, and a data recorder is available as an option. This recorder, referred to as the D*STAR system, is incorporated into a high-speed industrial computer, with a 2.3 Gbyte hard drive. This system is capable of directly storing up to 20 minutes of video data in real time, and it can then be used later to analyze the information.

Both of these cameras utilize miniature Sterling coolers for the detector, which avoids the use of liquid nitrogen. They are also compact, rugged, and operate quietly. The Inframetrics 760 was also

judged as being safer and less sensitive to movements than some of the competing scanned systems which use high-speed spinning polygonal mirrors.

2.3 AOTF AND ASSOCIATED POWER SUPPLY

The AOTF was designed to have a 1 inch aperture, a 2 cm^{-1} resolution, and an efficiency as high as possible. To achieve maximum resolution, a collinear AOTF must be used in order to maintain a reasonable aperture dimension, since a noncollinear design will greatly reduce the aperture due to vignetting associated with the off-axis geometry. The resolution of a collinear AOTF is given by

$$\Delta\lambda = 1.8\pi\lambda_o^2/(bL), \tag{28}$$

where, b2n, L is the interaction length, and $_o$ is the FWHM of the passband. With a resolution of $_o/_o^2 = 2$ cm^{-1}, the theoretical interaction length assuming perfect crystal quality is 2.2 cm.

For a transmission T_o through a collinear AOTF, the relationship for an ideal crystal is given by

$$T_o = \sin^2\left[\pi^2 M_2 I_a L^2/(2\lambda_o^2)\right]^{1/2} \tag{29}$$

where I_a is the acoustic intensity at the transducer, and M_2 is the acoustic figure of merit. At 10 μm with an interaction length of 2.2 cm, TAS will give 50% theoretical transmission efficiency at an acoustic intensity of 2.3 W/cm^2, which is a high, although practical value.

The field of view of a collinear AOTF is symmetrical in the polar and azimuthal directions, and the solid acceptance angle is given by $(_o/_o) = n^2$, which is identical to that of an etalon having a refractive index of n. At 10 μm and a resolution of 2 cm^{-1}, the FWHM acceptance angle for TAS is about 17.

A block diagram of the system control and rf power generation is shown in Figure 23, where the rf frequencies for the AOTF are produced by a SEITEQ ADS432-203 frequency synthesizer board, which is under the control of the computer through a VME controller. The temperature of the AOTF is also sensed by a thermistor, and adjustments are made in the rf frequency to compensate for temperature effects, which are needed to accurately track the spectra.

The temperature dependence of the AOTF passband can be obtained from the tuning curve, which is given approximately by

$$f_a = (V_a \Delta n/\lambda_o)(\sin^4\Theta_i + \sin^2\Theta_i)^{1/2}, \tag{30}$$

where V_a is the acoustic frequency, Δn is the birefringence, λ_o is the vacuum optical wavelength, and i is the design incidence angle. The temperature dependence is given by the derivatives

$$f_a/T = [f_a/(V_a n)](V_a n)/T, \quad (31)$$

and

$$\lambda_o/T = [\lambda_o/(V_a n)](V_a n)/T, \quad (32)$$

For the collinear design TAS AOTF, the numerical value is

$$f_a/f_a = \lambda_o/\lambda_o = -0.001145(T), \quad (33)$$

where T is in degrees Kelvin. Therefore at 10 μm, a 1.7 K temperature change will shift the passband by 2 cm^{-1}, which will require a compensating frequency change of 36 kHz.

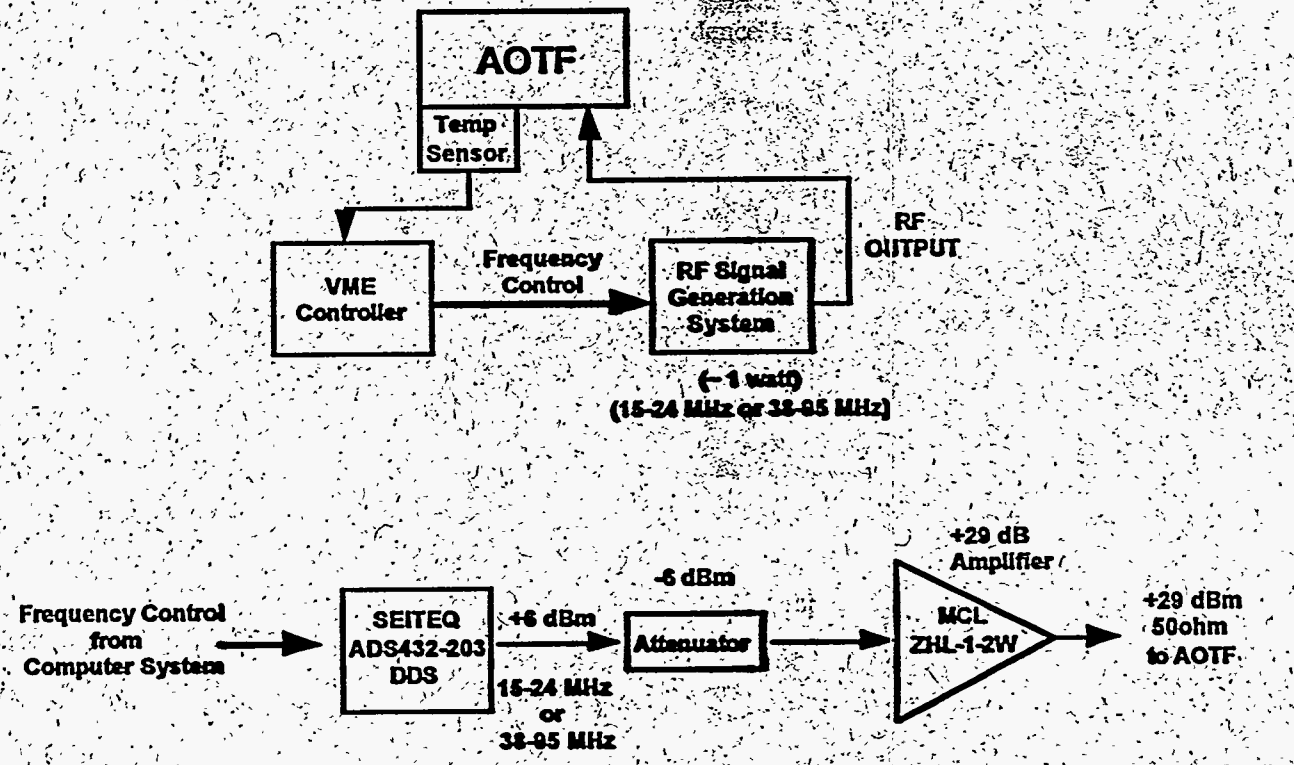

Figure 23 Block diagram of spectrometer control and rf generation subsystems.

2.4 SIGNAL PROCESSING AND SENSITIVITY ANALYSIS

After storing the image frames, the data will be processed at a rate of about 5-10% of the collection time. The basic processing procedure is to add frames and groups of pixels to increase the signal to noise (S/N), and then to difference the appropriate frames to obtain the spectral content. The S/N will increase as the square root of the number of added frames and pixels, and the temporal and spatial resolution will be degraded just enough through this procedure to obtain the required sensitivity. The locations of the species identified by this processing will then be identified on the original image by color dots, or other such identification. In this way, the gas species will be identified on a high resolution image scene.

The sensitivity of the system design was analyzed using the NET specified by the cameras, along with the AOTF and system parameters. This procedure is more direct than starting with basic system parameters, and gives a simpler, and generally more accurate analysis. The various system parameters, such as the detector D^* and camera field of view are all encompassed by the NET of the camera, and we can directly examine the sensitivity of a single pixel, and then apply the addition of frames and pixel groups to increase the sensitivity to the required level.

A temperature difference T must exist between the plume and the background being observed through the plume, and the attenuation through the plume is registered as a change in emissivity. Assuming the emissivity of the background is unity, the signal produced by a single camera pixel is[24]

$$S = R(A_d)()()x(T)L_b/T, \qquad (34)$$

where R is the responsivity of the detector element in volts/W, A_d is the detector area, is the system transmission, is the solid acceptance angle of the detector element, $exp(-x)$ is the transmission through the plume, and L_b is the blackbody spectral radiance in W/cm^2-sr-μm. The equivalent noise is given by

$$N = R(A_d)(T)(L_b/T)d, \qquad (35)$$

where T is the NET of the system, and the integral extends over the spectral coverage of the camera. The advantage of using NET is that R, , and A_d cancel in forming the S/N, which simplifies the calculation and and bases it on reliable system parameters.

The minimum sensitivity occurs with S/N = 1, and using the absorbances of the candidate gases at the specified tag lines, along with an AOTF efficiency of 10% at a resolution of 2 cm^{-1}, these minimum detectable levels were calculated. An integration time of 1 second per line was used, which is comparable to an FTIR spectrometer, which typically requires about 4 minutes of integration time to

cover the 8-12 μm range at a resolution of 2 cm^{-1}. The resolution was also degraded to a single pixel filling the entire image scene, which corresponds to the maximum sensitivity, and is also directly comparable to the FTIR, which has only a single point of resolution.

The sensitivity for a 60K temperature difference is shown in Table 12 for the 8-12 μm band, and the sensitivity for the 2-5 μm band under similar conditions is shown in Table 13. It can be seen that the 8-12 band predicts excellent sensitivities for a large number of the species, such as tributyl phosphate, but that the 2-5 μm band has a very limited number of species, and that the sensitivities are very poor. This is due to the blackbody curve falling off rapidly at shorter wavelengths, which for room temperature sources produces very little optical power below 3.5 μm. Heavy molecules also tend to have a much better spectra in the 8-12 μm region, which limits the species available in the 2-5 μm band to lighter molecules.

Table 12. Predicted detection sensitivities of various candidate gases in the 8-12 μm region.

Chemical Name	, um	Absorbance	Width, cm^{-1}	(ppb-m)
Tributyl phosphate	9.680	5.684	43.6	16
Carbon tetrachloride	12.582	5.144	55.4	18
Nitrous acid	11.731	2.829	7.4	32
Trichloroethylene	11.772	0.902	33.9	100
Ammonia	10.741	0.841	22.9	110
Dichlorodifluoromethane	13.092	0.764	30.9	120
Methanol	9.678	0.721	9.7	130
m-Xylene	13.020	0.525	30.3	170
Nitric acid	11.382	0.467	4.0	200
Di + Monobutyl phosphate	9.608	0.409	2.1	220
p-Xylene	12.575	0.351	48.7	260
2-Butanone	8.552	0.298	2.8	310
Butanol	9.349	0.206	83.0	450
Hydrazine	10.631	0.196	10.3	470
Nitrogen tetroxide	12.940	0.083	2.0	1,100
4-methyl 2-Pentanone	8.877	0.072	14.6	1,300
Sulfur dioxide	8.597	0.069	3.2	1,300
Benzene	9.639	0.066	46.7	1,400

Table 13. Predicted detection sensitivities of various candidate gases in the 2-5 μm region.

Chemical Name	um	Absorbance	Width, cm^{-1}	(ppb-m)
Methane	3.314	0.738	25.8	4,500
Dodecane	3.514	0.135	4.5	14,000
o-Xylene	3.361	0.182	16.1	16,000
Hydrogen cyanide	2.999	0.232	2.8	44,000
Hydrogen fluoride	2.499	0.741	5.9	160,000

Due to the poor predicted performance in the 2-5 μm band, it is recommended that the spectrometer should concentrate only on the 8-12 μm band. This band uses the Inframetrics 760 camera, for which there is available the Inframetrics D*STAR System, which is an industrial computer that can store up to 20 minutes of real-time video data from the camera on a very large drive. This computer can then be used to process the stored data, and it can also be used to control the AOTF during the data acquisition.

3. REFERENCES

1. E. J. McCartney, Absorption & Emission by Atmospheric Gases, John Wiley & Sons, New York (1983).

2. P. L. Hanst and S. T. Hanst, Infrared Spectra for Quantitative Analysis of Gases, Infrared Analysis.

3. P. L. Hanst and S. T. Hanst, Gas Measurement in the Fundamental Infrared Region, Infrared Analysis.

4. S. Wold, H. Martens, and H. Wold, "The Multivariate Calibration Problem in Chemistry Solved by the PLS Method," 286, Proc. Conf. Matrix Pencils, A. Rhue, B. Kagstrom, Eds., Springer Verlag, Heidelberg (1983).

5. D. W. Marquardt, "An Algorithm for Least-Squares Estimation of Nonlinear Parameters," J. Soc. Ind. Appl. Math. 11: 431 (1963).

6. A. Savitzky and M. J. E. Golay, "Smoothing and Differentiation of Data by Simplified Least Squares Procedures," Anal. Chem. 36: 1627 (1964).

7. H. Press, B. P. Flannery, S. A. Teukolsky, and W. T. Vetterling, Numerical Recipes, 2nd Ed., Cambridge University Press, New York (1992).

8. R. T. Menzies, "Laser Heterodyne Detection Techniques," Chap. 7, Laser Monitoring of the Atmosphere, E. D. Hinkley, Ed., Spring-Verlag, New York (1976).

9. H. R. Carlon, "The Apparent Dependence of Terrestrial Scintillation Intensity upon Atmospheric Humidity," Appl. Opt. 4: 1089 (1965).

10. J. A. Fox, C. R. Gautier, and J. L. Ahl, "Practical Considerations for the Design of CO_2 Lidar Systems," Appl. Opt. 27: 847 (1988).

11. J. F. Schultz, Los Alamos National Laboratory (Private Communication).

12. A. J. LaRocca, "Atmospheric Absorption," Chap. 5, The Infrared Handbook, W. L. Wolfe and G. J. Ziessis, Eds., U.S. Government Printing Office, Washington (1978).

13. H. A. Gebbie, W. R. Harding, C. Hilsum, A. W. Pryce, and V. Roberts, "Atmospheric Transmission in the 1 to 14 μm Region," Proc. R. Soc. London A206: 87 (1951).

14. G. P. Anderson, S. A. Clough, F. X. Kneizys, J. H. Chetwynd, and E. P. Shettle, "AFGL Atmospheric Constituent Profiles (0-120 km)," Air Force Geophysics Laboratory Report AFGL-TR-86-0110 (1986).

15. P. H. Howard and M. Neal, Dictionary of Chemical Names and Synonyms, Lewis Publishers, Ann Arbor (1992)

16. N. B. Colthup, L. H. Daly, and S. E. Wiberley, Introduction to Infrared and Raman Spectroscopy, Academic Press, New York (1964).

17. Lab Calc User's Guide, Galactic Industries Corp. (1993).

18. R. L. Byer, "Review: Remote Air Pollution Measurement," Opt. & Quantum Electron. 7: 147 (1975).

19. C. L. Wyatt, Radiometric System Design, Macmillan Pub. Co., New York (1987).

20. EG&G Judson Optoelectronics 1994 Infrared Detectors Catalog.

21. S. S. Penner, Quantitative Molecular Spectroscopy and Gas Emissivities, Addison-Wesley Pub. Co. (1959).

22. F. Daniels and R. A. Alberty, Physical Chemistry, John Wiley & Sons, New York (1955).

23. CRC Handbook of Chemistry and Physics, 75th Ed., R. C. Weast, Ed., CRC Press, Boca Raton (1994).

24. D. F. Flanigan, "Detection of Organic Vapors with Active and Passive Sensors: a Comparison," Appl. Opt. 25: 4253 (1986).